Optical readout tracking detector concept using secondary scintillation from liquid argon generated by a thick gas electron multiplier

2009 JINST 4 P04002

(http://iopscience.iop.org/1748-0221/4/04/P04002)

PUBLISHED BY IOP PUBLISHING FOR SISSA

RECEIVED: *December 11, 2008*
REVISED: *February 27, 2009*
ACCEPTED: *March 8, 2009*
PUBLISHED: *April 1, 2009*

Optical readout tracking detector concept using secondary scintillation from liquid argon generated by a thick gas electron multiplier

P.K. Lightfoot,[a,1] **G.J. Barker,**[b] **K. Mavrokoridis,**[a] **Y.A. Ramachers**[b] **and N.J.C. Spooner**[a]

[a] *Department of Physics and Astronomy, University of Sheffield, Hicks Building, Hounsfield Road, Sheffield, S3 7RH, U.K.*
[b] *Department of Physics, University of Warwick, Coventry, CV4 7AL, U.K.*

E-mail: p.k.lightfoot@sheffield.ac.uk

ABSTRACT: For the first time secondary scintillation, generated within the holes of a thick gas electron multiplier (THGEM) immersed in liquid argon, has been observed and measured using a silicon photomultiplier device (SiPM).

250 electron-ion pairs, generated in liquid argon via the interaction of a 5.9 keV Fe-55 gamma source, were drifted under the influence of a 2.5 kV/cm field towards a 1.5 mm thickness THGEM, the local field sufficiently high to generate secondary scintillation light within the liquid as the charge traversed the central region of the THGEM hole. The resulting VUV light was incident on an immersed SiPM device coated in the waveshifter tetraphenyl butadiene (TPB), the emission spectrum peaked at 460 nm in the high quantum efficiency region of the device.

For a SiPM over-voltage of 1 V, a THGEM voltage of 9.91 kV, and a drift field of 2.5 kV/cm, a total of 62 ± 20 photoelectrons were produced at the SiPM device per Fe-55 event, corresponding to an estimated gain of 150 ± 66 photoelectrons per drifted electron.

KEYWORDS: Scintillators, scintillation and light emission processes (solid, gas and liquid scintillators), Cryogenic detectors, Liquid detectors, Calorimeters

[1] Corresponding author.

doi:10.1088/1748-0221/4/04/P04002

2009 JINST 4 P04002

Contents

2009 JINST 4 P04002

1 Introduction

The liquid argon time projection chamber (TPC) is a leading technology candidate for the type of large scale underground detector widely acknowledged to be the next-generation project in the areas of neutrino oscillation physics, astro-particle physics and proton decay. The current challenge is to build on the proof-of-principle achievements of the ICARUS program [1] to establish methods of tracking and homogeneous calorimetry that combine the excellent performance of a liquid argon TPC with a practical implementation that is cost effective and readily scalable up to the benchmark of 100 kton.

Charge losses over long drift distances in liquid argon mean that amplification of charge is required. Gas electron multipliers (GEMs) [2], THGEMs [3], Micromegas [4], and Bulk Micromegas [5], have evolved over the last 20 years and are now routinely used within large volume

targets due to their high spatial resolution, small thermal mass and physical size, low radioimpurity concentration and flexible read-out configuration. Significant charge amplification within the liquid has proven difficult to achieve in a practical design [6] leading to the consideration of two-phase liquid argon volumes where the charge amplification using GEM's or THGEM's occurs in the gas phase above the liquid volume. Examples of previous research in this field are contained in references [7]–[9]. These designs bring their own problems however and there is a risk the performance could be compromised on the largest scales by the requirements of precise liquid levelling, extreme cooling stability and space-charge effects at the liquid-gas interface.

There is motivation therefore to investigate alternative ways in which a single phase liquid argon volume could be used for 3D tracking and in particular the possibility of using scintillation light readout rather than charge. We report on a feasibility study into observing the secondary scintillation light, or luminescence, generated from within the holes of a THGEM plane placed at the edge of a drift volume initiated by the ionisation charge deposited in the volume. An array of photo-sensors mounted behind the THGEM plane could then 'image' the light signal by reconstructing the centroid of the light emission in the XY plane and using the electron drift velocity within liquid argon to give the drift coordinate. This work builds on an earlier study in which we demonstrated that SiPM devices were a suitable choice of photo-sensor to operate in the liquid argon volume [10] and which brought advantages over conventional PMT's. Most importantly, the total decoupling of the optical readout device from the electrical systems (e.g. drifting charge, transfer fields and readout system) promises a tracking module with superior noise performance.

The successful operation of single phase liquid argon TPC's based on light readout via, for example the imaging of THGEM planes with SiPM arrays, would significantly reduce the complexity of design and allow modular construction of large arrays with readout in any plane. This report describes the first measurement of secondary scintillation light produced within the holes of a THGEM and viewed by a SiPM device all within a single phase liquid argon target.

2 Experimental details

2.1 Experimental apparatus

The apparatus, shown in figure 1, used in all measurements consisted of an inner steel test chamber of height 550 mm and diameter 98 mm held within a concentric outer chamber of height 750 mm and diameter 250 mm. Both chambers were contained within a copper vacuum vessel and access to each chamber was provided through tubes in an exterior top flange of diameter 420 mm. The internal assembly, shown in figure 2, consisted of a 1 mm^2 SiPM device[1] positioned directly above the centre of a 65 mm diameter THGEM, located above a 20 mm drift region defined by a woven steel cathode at the base of the assembly. Two parallel plate capacitors, positioned to the side of the device, acted as level sensors, the change in the overall capacitance determined by the phase of the argon dielectric indicating that the liquid level was either above or below each position. This entire arrangement was fixed to two stainless steel support rods and positioned close to the base of the target chamber.

[1] SPM1000 device from SensL Technologies Ltd., Cork, Co Cork, Ireland

2009 JINST 4 P04002

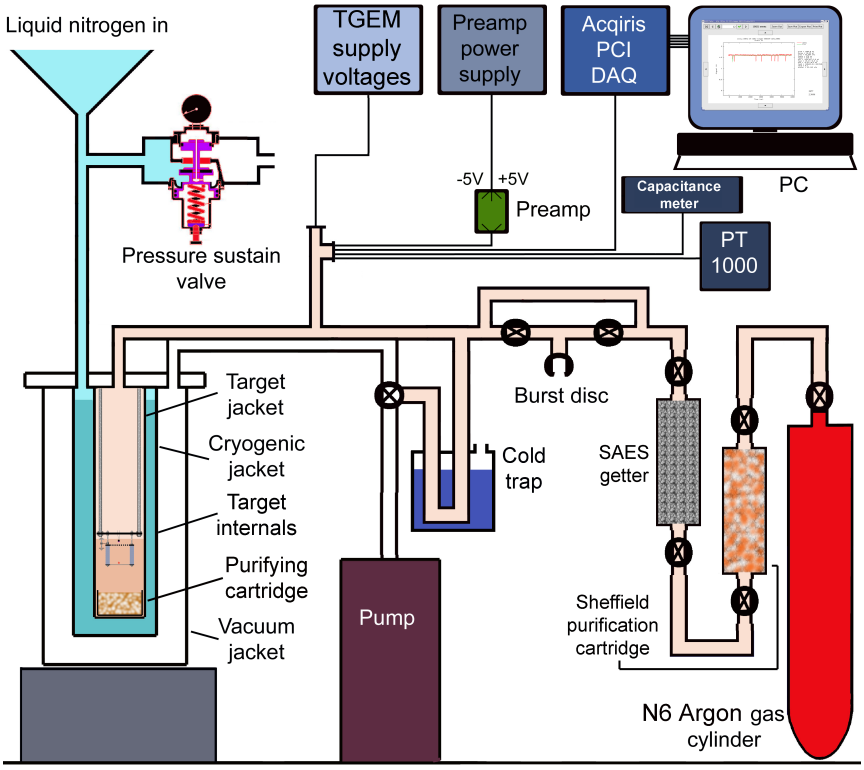

Figure 1. Experimental apparatus, ancillary equipment, and data acquisition system.

The THGEM was manufactured from a double faced copper clad FR-4 epoxy resin glass reinforced composite plate of thickness 1.5 mm, hole diameter 1 mm, pitch 1.5 mm. Only the central 45 mm diameter region of the THGEM was perforated, all copper etched from the outer radius to limit effects such as corona discharge which would otherwise increase the probability of discharge sparking. No dielectric rims were etched around the THGEM holes. On completion of CNC machining, the THGEM was immersed in 10 M nitric acid to smooth surface irregularities. To avoid frequent removal of the THGEM from the acid, washing with deionised water, and viewing under a microscope, two devices were etched simultaneously, one device being removed and assessed as an indicator for the extent of etching on the other device which remained in the acid undisturbed throughout. On conclusion a visual assessment was made of the randomness of the sparking produced during high voltage breakdown in air.

The THGEM was attached to the drift region below, and to the SiPM device above, using long polypropylene bolts as shown in figure 2. The SiPM device was shielded from the field within the THGEM by a grounded high optical transparency woven steel mesh grid, positioned between the THGEM and the SiPM device in order to deflect electrons passing through the THGEM holes back towards the THGEM top electrode, each hole acting as an independent amplifier. The optical transparency of the THGEM is defined in equation 1 in which D is the diameter of the hole and P is the pitch. The transparency of the THGEM was 40%. In addition two 5 mm diameter polystyrene cylinders were fitted between the SiPM and the THGEM to isolate the SiPM device

2009 JINST 4 P04002

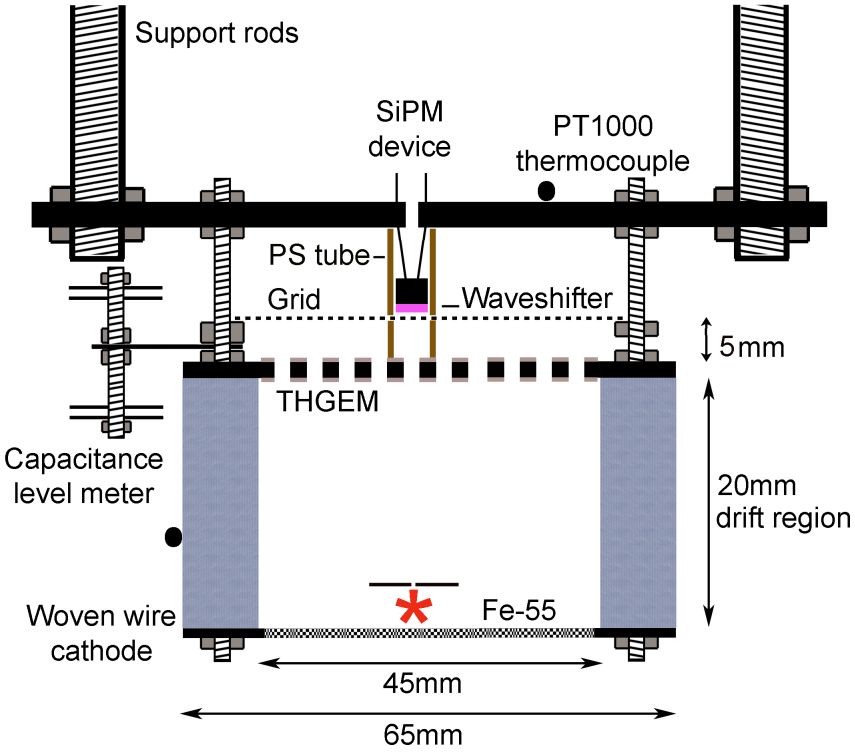

Figure 2. Internal assembly used to detect secondary scintillation in liquid argon.

from background scintillation light from the argon target as shown in figure 2.

$$T = \frac{\pi D^2}{P^2\sqrt{12}} \tag{2.1}$$

Although the principle aim was the measurement of secondary scintillation from liquid argon using the SiPM device, satisfactory performance of the THGEM was first confirmed by reading out the charge produced in the gas phase at room temperature. In all cases the bottom face of the THGEM was grounded, a drift field between 1 and 4 kV/cm created by applying negative potential to the steel cathode using a Caen N470 8 kV power supply. The amplification field within the THGEM was controlled through a 10 MΩ protection resistor at the top THGEM electrode using a 30 kV Wallis high voltage supply through a 20 kV rated feedthrough in the target housing. The charge signal, read from the top THGEM electrode, was decoupled from the high voltage line through a 47 pF capacitor and passed through an Amptek A250 charge sensitive preamplifier, an Ortec 572 shaping amplifier with gain set to $\times 50$ and a shaping time of 2 μs, to an Acqiris CC108 PCI acquisition system triggered through a discriminator unit. Software recorded all events and calculated the mean and standard deviation of the pulse height, displaying a histogram of the distributions.

The gain of the THGEM was defined as the charge after the avalanche stage divided by the initial charge prior to amplification. Since 250 electron-ion pairs are created in every Fe-55 interaction in argon a total charge of 4×10^{-17} C is assumed to be transferred through the drift region towards the THGEM. A Canberra 2003BT charge to voltage pre-amplifier known to convert 1pC into a 450mV signal was connected to the top THGEM electrode and the voltage at the Canberra

2009 JINST 4 P04002

Table 1. Characteristics of SensL series 1000 SiPM device and associated pre-amp.

Pixel size	**Number of cells**	**Geometric efficiency%**	**Maximum gain**	**Pixel recovery time**	**Spectral range (nm)**	**$V_{breakdown}$ at 25°C**
20 μm	848	43	8×10^6	40 ns	400 - 700	28.2 V

unit recorded as the potential difference was increased across the THGEM. The charge present following amplification was measured using the conversion factor above, and the gain was therefore calculated. A pulser was used to verify calibration of the Canberra unit and to confirm that it produced a linear amplification response with increased input charge. In all future measurements it was then possible to convert peak position in Vns to gain.

The optical signal was readout using a SensL series 1000 SiPM connected to an external preamplifier powered using a Digimess DC power supply HV3003-2, the bias voltage supplied by a Thurlby Thandor PL320 32 V, 2 A DC supply with sense active. Device characteristics are listed in table 1. The output signal from the SiPM preamplifier was split, one signal passing directly to an input channel on the Acqiris unit. The other signal was connected through an Ortec 572 shaping amplifier with a 10 μs integration time, to a N417 discriminator and then to the trigger input of the Acqiris unit.

Prior to all tests the inner chamber was evacuated to 1×10^{-8} mbar and baked to 60 °C. For all low temperature measurements as liquid nitrogen was slowly added to the cryogenic jacket, the pressure of argon gas within the target was maintained at 1 bar until liquefaction eventually occurred. At this point the cryogenic jacket was filled with liquid nitrogen and pressurized to between 3 and 3.5 bar thereby increasing the boiling point of liquid nitrogen to the point at which liquid argon could condense within the target at 1 bar. In all tests the target was connected to a bursting disc rated at 2.2 bar to protect against over pressure within the apparatus in the event of a cooling failure.

PT1000 platinum resistance thermocouples attached to the SiPM support platform and drift region provided accurate temperature information, and careful addition of liquid nitrogen to the cryogenic jacket enabled the temperature of the assembly to be stabilized for any time to an accuracy of $\pm1\,^{\circ}$C. The only thermal inputs were radiation from the walls and conduction along the support structure and power lines. All power supplies were connected to the same electrical supply to ensure a common ground which was then routed through a transformer. Kapton insulated UHV coaxial cables were used for all internal connections and the signal transfer lines from the SiPM device to the external preamplifier were further shielded with stainless steel braid earthed to the chamber wall.

2.2 Purification of argon

Increased target mass and longer drift lengths impose ever greater requirements on the construction and operation of ultra pure liquid noble gas targets, electronegative impurities within the argon reducing the electron lifetime and therefore the charge transfer efficiency across the drift region.

2009 JINST 4 P04002

Impurities within liquid argon can also absorb emitted UV photons or quench argon excimers, leading to a loss of light collection, an impurity concentration of 500 ppb nitrogen in liquid argon reducing the triplet lifetime by 0.1 μs [11].

The electron drift velocity in liquid argon has been accurately measured as a function of the electric field, the drift velocity being 2 mm/μs within a 1 kV/cm field, increasing to 5 mm/μs in a 10 kV/cm field [12]–[14]. The approximate electron lifetime is given by equation (2.2) [15, 16].

$$\text{Electron lifetime } \tau \approx 300\mu s \times \frac{1\,ppb}{[LAr\ purity\ in\ ppb]} \tag{2.2}$$

For an electron to transit 20 mm within a 1 kV/cm drift field, a liquid purity of at least 30 ppb is required. The highest purity industrial argon is N6 (1 impurity part per million) from BOC Special Gases Ltd,[2] necessitating additional purification to achieve the required level of less than 30 ppb. N6 gaseous argon was first passed from its cylinder through a purification cartridge containing a 1200 g blend of powdered copper and phosphorous pentoxide to remove the bulk of oxygen and water respectively. The argon gas was then passed through a SAES[3] getter (model number PS11-MC1-R) at a flow rate of 5 L/min at 1.2 bar to remove oxygen and water to less than 1 ppb. To allow continued removal of impurities such as physisorbed water from within the target during operation, an additional purification cartridge was positioned at the base of the chamber directly below the target assembly as shown in figure 1. In addition to copper and phosphorus pentoxide, this cartridge contained both 13X and 5Å molecular sieves to remove mineral oil, turbo and rotary pump oil. To eliminate back flow from the pumping system a liquid nitrogen cold trap was also placed between the turbomolecular pump and the target as shown in figure 1.

2.3 Waveshifter coating of the SiPM device

Argon emits VUV scintillation light at 128 nm. The photon interaction depth in silicon is 1 μm for 440 nm light and 5 nm for 172 nm light [17] so UV photons interact in the first atomic layers where the electric field is weaker and the impurity concentration is higher with the effect that the quantum efficiency is reduced. Light collection can be increased by coating the SiPM device with a waveshifter to shift direct 128 nm VUV light to 460 nm visible light [18] and therefore into the sensitive high quantum efficiency region of the device [10]. Application of the waveshifter via evaporation or spraying was rejected since the coating was considered impossible to remove without applying damaging solvents to the SiPM window. A 50% concentration of the waveshifter tetraphenyl butadiene (TPB) in a mineral oil based diblock copolymer elastomer with 10% toluene and 3 % plasticizer was therefore applied to the SiPM face. This had the consistency of a gel and could be easily removed by peeling, separate evaluation using a coated low temperature PMT revealing consistent shifting efficiency to -196 °C.

2.4 Source selection

Selection of an appropriate radiation source was based on the requirements that not only should a high percentage of photons interact in the drift volume in both gas and liquid, but that the electron

[2]BOC Limited, Guildford, Surrey, United Kingdom
[3]SAES Getters Group, Lainate, Lombardy, Italy

2009 JINST 4 P04002

Table 2. Scintillation time constant characteristics of argon.

Singlet time constant (ns) in gaseous argon [21]	**Triplet time constant (ns) in gaseous argon** [23]	**Singlet time constant (ns) in liquid argon** [20]	**Triplet time constant (ns) in liquid argon** [20]
11.3	3140	6	1590

created via the photoelectric effect should have a range less than the width of a THGEM hole to ensure full capture of the event. The choice of a single source for both room temperature and low temperature operation allowed continuous gain to be measured across the performance envelope without opening the target and destroying purity. Fe-55 (5.9 keV gamma emitter) was selected and positioned at the centre of the steel woven cathode within the drift region, the source collimated using a thin steel sheet to ensure gamma interactions were limited to the vertical axis through the SiPM device.

In 1 bar gaseous argon at room temperature 61% of the gammas interact within the drift region, producing a corresponding electron track length of 0.6 mm, whereas in liquid argon 100% of the gammas interact, the electron track length being 70 μm. The average number of primary electrons-ion pairs generated from a 5.9 keV Fe-55 source assuming a W-value of 23.6 eV [19] was 250. The ratio of the charge collected at the top THGEM electrode or the number of secondary photons detected by the SiPM to the charge generated within the drift region was then used to determine the charge gain and optical gain respectively of the THGEM when operated in charge amplification mode or scintillation mode. The average event rate due to the source was determined from its half life, age, and the extent of collimation to be 6 kHz. The long triplet time constant necessitates the use of extended data acquisition integration windows up to 10 μs, and it was considered essential to select a source of low activity to avoid pulse pile-up.

2.5 Scintillation characteristics of argon

Key liquid argon properties are shown in table 2. Excitation leads to the creation of both singlet and triplet excimers, scintillation due to the transitions from these states to the ground state then characterised by the presence of two exponentials with different time constants [20, 21]. The ratio of the fast singlet state $^1\Sigma_u^+$ to the slow triplet state $^3\Sigma_u^+$ is 0.3 for electron recoils in liquid argon [22]. This ratio is only weakly dependent on the energy of the electron recoil and is essentially constant in the 0-150 keV range [22]. In room temperature gaseous argon the ratio of the fast singlet state $^1\Sigma_u^+$ to the slow triplet state $^3\Sigma_u^+$ is approximately 2 for electron recoils. This figure has been deduced by the authors of this report by fitting the respective decay times to pulses generated following gamma interaction with gaseous argon, and calculating the ratio of the areas under each integrated exponential fit.

3 Results

Below is a detailed account of the results obtained operating a SiPM device and THGEM in room temperature gaseous argon, in the vapour phase above double phase argon, and fully immersed

2009 JINST 4 P04002

in liquid argon using the assembly shown in figure 2 within the apparatus shown in figure 1. In order to fully characterise the assembly, it was essential initially to both measure the performance limitations of the SiPM device and ensure that the THGEM was operating correctly. Following this, the field within the THGEM was varied and secondary scintillation measured as a function of the THGEM field using the SiPM device.

3.1 Limit of SiPM device linearity due to saturation effects at high LED photon flux rates

Due to the digital nature of operation, at any time a proportion of the total number of pixels of the SiPM device will be in a state of recovery, the absolute number dependent on the intensity and frequency of the photon flux and to a lesser extent on the dark count rate. This characteristic places a limit on the extent of linearity of the device especially for high intensity pulses of similar time scale to the recovery time.

For electron recoils within liquid argon approximately 23% of all photons are produced within the first 6 ns following an interaction, the remaining 77% forming an exponential distribution with a 1590 ns time constant [20]. Because of the extended decay time compared with for example xenon, SiPM devices are well matched to liquid argon targets since the total signal duration is far in excess of the pixel recovery time. It is however crucial that the SiPM device contain a sufficient number of pixels in order to retain a linear response to the fast singlet component, and characterisation of the SiPM response with increasing photon flux is therefore essential.

An evaluation of the linearity of the output signal from the SiPM with increasing light intensity was performed at -196 °C. Full experimental details are contained in reference [10]. A pulsing circuit based on that of Kapustinsky [24] was connected to an externally mounted light emitting diode (LED) producing 5 ns rise-time 15 ns decay-time light pulses of variable intensity, which were passed through a fibre optic cable to the SiPM device held on a support structure within the target. Saturation of the SiPM device is a function of the photon detection efficiency (PDE) and therefore the over-voltage, the light intensity and the pulse frequency. In all tests the pulse frequency was maintained at 100 Hz, the LED photon flux calibrated using an ETL D749QKFLA PMT. For a fixed over-voltage, the intensity of the 460 nm LED pulse was gradually increased from 20 photons to the point at which the output signal became clipped by the preamplifier. The over-voltage was then increased and the procedure repeated.

Measurements have shown linearity of the output signal is maintained at low incident photon fluxes irrespective of the over-voltage. Data shown in figure 3 indicates a 5% deviation from linearity to occur for a 1 V over-voltage for incident fluxes containing in excess of 1500 photons, whereas for a 2 V over-voltage a 5% deviation is observed for fluxes in excess of 350 photons. A 1.5 V over-voltage remains linear within 5% until a flux of approximately 650 photons. However, although linearity is preserved over a large dynamic range, the PDE for a 1.0 V over-voltage is only 5.6%, a 20 ns LED pulse containing 234 photons yielding only 12.8 photoelectrons, whereas an identical signal yields 36.8 photoelectrons at 2.0 V over-voltage. In all future measurements using argon each scintillation pulse was assessed to ensure that the photon flux within any 40 ns window did not exceed the stated 5% deviation limit for the selected over-voltage value.

2009 JINST 4 P04002

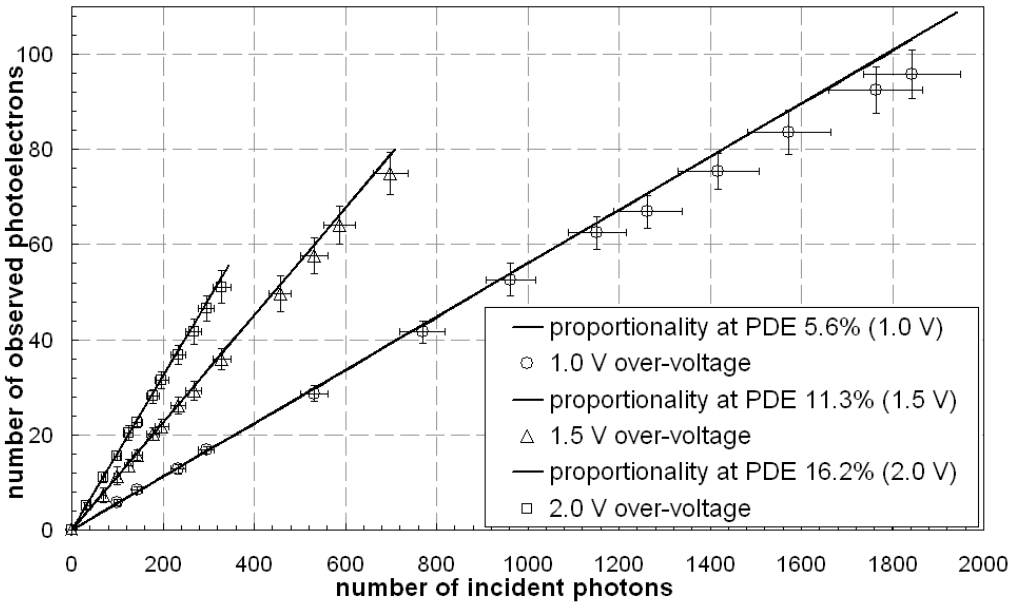

Figure 3. Linearity of a SiPM device at high LED photon flux rate.

3.2 Room temperature operation of the THGEM in charge amplification mode in gaseous argon

Initial testing of the 45 mm diameter, 1590 mm^2 active area THGEM, evaluated its performance envelope in room temperature purified argon gas. The effect of increasing the amplification field within the THGEM on the charge gain was evaluated over a range of pressures as shown in figure 4. The effect on the gain as a consequence of increasing the drift field for a constant amplification field was also measured as shown in figure 5. Results indicate that for a fixed amplification field corresponding to a THGEM potential of 2.55 kV, no improvement in charge collection occurs for drift fields in excess of 0.6 kV/cm in 20 °C 1 bar argon.

In 1 bar gaseous argon at room temperature 61% of the gammas interact within the drift region, producing a corresponding electron track length of 0.6 mm Collimation of the gamma source ensures that gammas entering the drift region are mainly directed towards the central THGEM hole. Coupled with the fact that the electron track length is shorter than the THGEM hole diameter and diffusion is low over such short distances, efficient capture of the event is expected. To protect the THGEM from damage caused by dielectric surface breakdown, measurements were discontinued once the current between the THGEM electrodes became unstable although evidence of erratic charge gain was noted at high voltages and very gradual adjustment of the voltage was essential.

3.3 Room temperature measurement of secondary scintillation generated within a THGEM in gaseous argon using a SiPM device

The SiPM device positioned 5 mm above the THGEM, as shown in figure 2, was operated at an over-voltage of 1 V corresponding to a gain of 5×10^5 [10], a single photoelectron area of 0.5 Vns, and a PDE of 5.6% [10]. For a constant drift field of 1 kV/cm, the electric field between the

2009 JINST 4 P04002

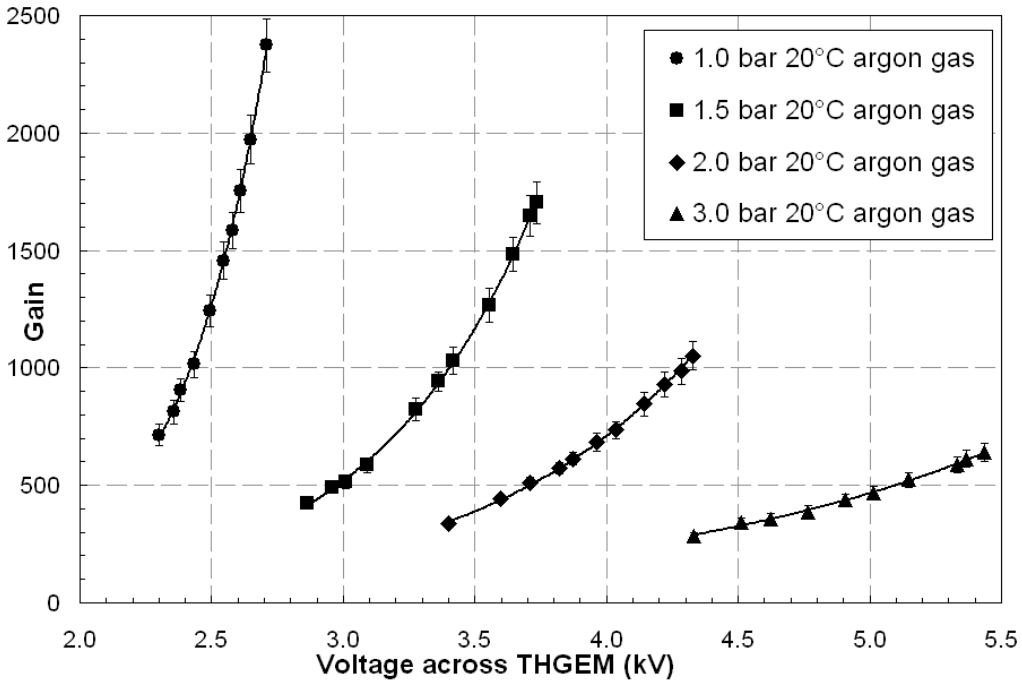

Figure 4. Charge gain versus potential across THGEM for a 1 kV/cm constant drift field.

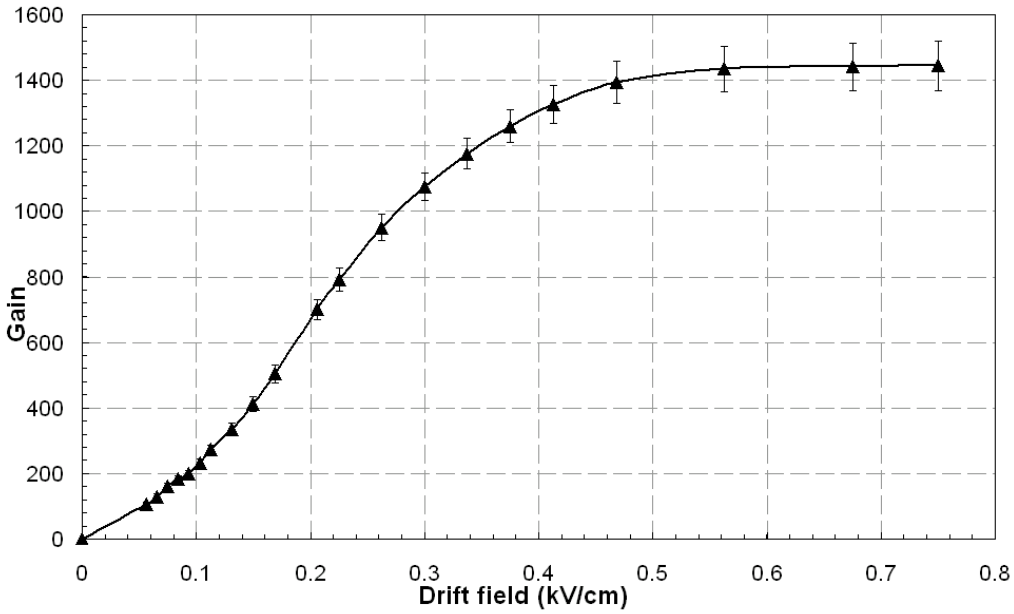

Figure 5. Charge gain versus drift field in 20 °C 1 bar argon for a fixed THGEM potential of 2.55 kV.

THGEM electrodes was steadily increased. With reference to figure 5 the degree of charge collection is identical for a drift field of 1 kV/cm compared to a drift field of 0.75 kV/cm. The SiPM signal, as already detailed, was split to enable a simultaneous trigger pulse from a discriminator unit.

2009 JINST 4 P04002

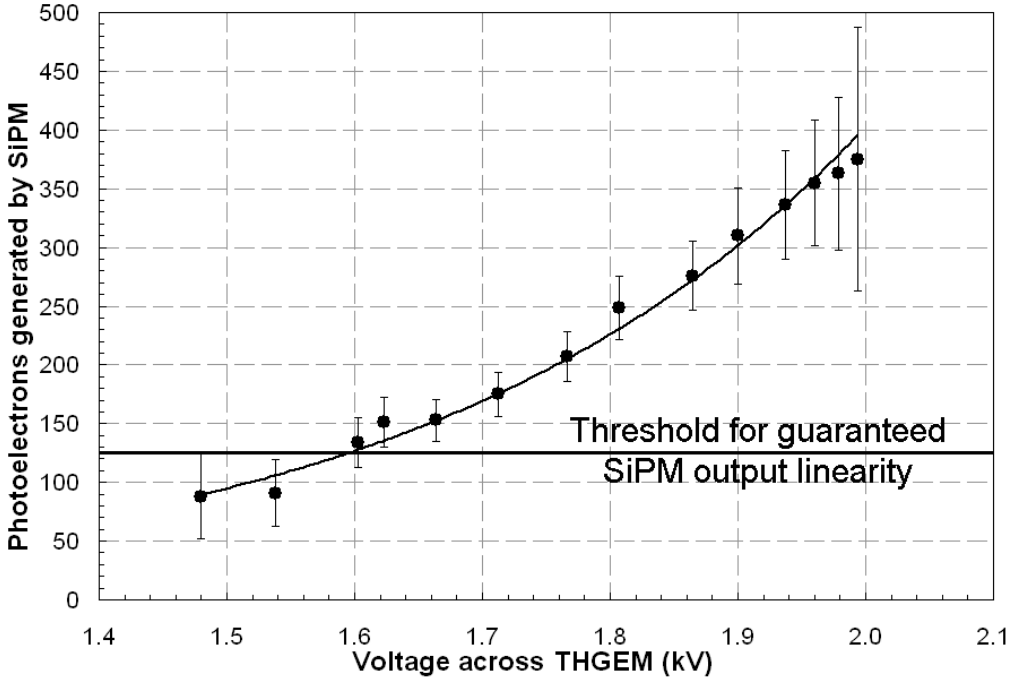

Figure 6. Secondary scintillation in 1 bar 20 °C gaseous argon as a function of the voltage across a THGEM due to the passage of charge generated via the interaction of an Fe-55 source within a constant 1 kV/cm drift field.

The number of photoelectrons registered at the SiPM was then determined via off-line integration of the acquired pulse following the initial trigger. The dark count rate (DCR) at room temperature and for an over-voltage of 1 V has been measured as 350 kHz [10] corresponding to an average of 4 DCR events within a 10 μs window. With both THGEM electrodes grounded a measurement was first made of the photoelectron background contribution due to argon scintillation within the small volume of the polystyrene tube. Neglecting very infrequent pulses containing in excess of 100 photoelectrons, the average distribution contained less than 35 photoelectrons within the 10 μs window. As the field within the THGEM holes was increased, the sudden onset of secondary scintillation, characterised by the distinctive argon scintillation pulse containing a significant number of photons, was observed at 1.48 kV. As the THGEM voltage increased no linearity was observed between the voltage applied to the THGEM and the number of photoelectrons generated, the rate of VUV photon production increasing exponentially even beyond the point at which the SiPM device became saturated. Figure 6 shows light collection as a function of the voltage across the THGEM. The threshold for guaranteed SiPM output linearity is defined from analysis of the data as the point at which a pulse contains in excess of 84 photoelectrons within any 40 ns time period.

By comparing figures 4 and 6, the nature of the secondary scintillation process can be deduced. During charge multiplication an electron drifting in an elevated electric field gains sufficient energy to ionise the atoms of the medium. These electrons then interact, producing additional ionisation and therefore an exponential scaling with applied field (see figure 4). Secondary scintillation scales linearly with increasing field [25] within the THGEM because unlike charge multiplication, the

2009 JINST 4 P04002

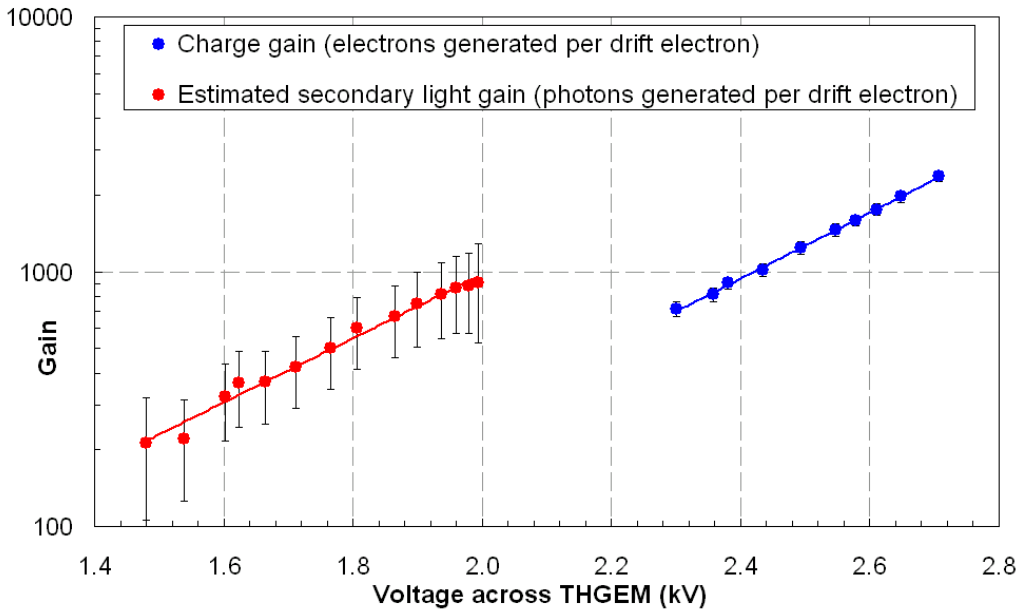

Figure 7. Estimated secondary scintillation gain and charge gain in 1 bar gaseous argon as a function of voltage across the THGEM.

energy of the drifting charge is dissipated via the emission of UV photons which do not participate further in the process. However in room temperature gaseous argon no clear secondary scintillation signal is observed until the THGEM is clearly operating in the charge multiplication regime, the exponential multiplication of charge initiating a corresponding exponential increase in the degree of secondary scintillation light (see figure 6). This effect has previously been observed in room temperature xenon using GEMs [26] and may also be attributed to poor focussing of field lines passing from the drift region into the THGEM holes at the low fields sufficient to generate secondary scintillation.

The absolute photon yield per drifting electron can be ascertained by considering the efficiency of transfer between each stage. Although very approximate, this is a fundamental parameter for any secondary scintillation based detector. The efficiency of charge transfer passing from the drift region inside the holes was estimated as 80% $\pm$ 10% based on measurements detailed within a separate report [27]. The solid angle presented by the SiPM was 8% $\pm$ 1%, and the optical transparency of the protection grid was 64% $\pm$ 4%. The global TPB waveshifting efficiency and the attenuation length within the gel was measured at 7% $\pm$ 6% and the PDE of the SiPM device at 1 V over-voltage was 5.6% $\pm$ 1.2% [10]. The scintillation yield in terms of photons generated at the THGEM per drift electron as a function of the voltage between the electrodes is shown in figure 7 and compared with the charge gain.

3.4 Cryogenic operation of the THGEM in charge amplification mode in the vapour phase of a double phase argon system

Having verified correct operation of both the THGEM and SiPM device in room temperature gaseous argon, liquid argon was condensed within the chamber and the THGEM operated once

2009 JINST 4 P04002

again in charge gain mode in order to confirm that both the magnitude of the drift field and the degree of purification were sufficient to enable charge transfer through the liquid. A level sensor consisting of two parallel plate capacitors connected in parallel was positioned as shown in figure 2. During liquefaction the capacitance of the level sensor, measured using an Agilent 4263B LCR meter, was 44 pF in 1 bar saturated argon gas, 57 pF once the liquid level was at a specific position above the source but below the THGEM, and 70 pF once the SiPM and THGEM were both submerged. Once the appropriate capacitance value had been reached, the gas inlet valve was closed and the pressure within the target maintained at 1 bar via adjustment of the pressure within the liquid nitrogen filled cryogenic jacket.

The dielectric constant ε is 1.6 for liquid argon and 1.000574 for gaseous argon. Used to provide level sensing, this also affects the field within the drift region. For a total voltage ΔV applied between the bottom THGEM electrode and the cathode, the electric field in both the liquid (E_L) and gas (E_G) are related to the depth of the liquid (d_L) and the height of the gaseous region (d_G) by the equations below.

$$E_G = \varepsilon\, E_L \tag{3.1}$$

$$E_L = \frac{\Delta V}{(\varepsilon\, d_G + d_L)} \tag{3.2}$$

The electron extraction probability depends on the strength of the electric field across the gas liquid interface. Charge extraction across the liquid gas boundary has been shown to be complete at fields within the liquid phase of 3 kV/cm [28]–[31]. The lower capacitor was positioned to enable the liquid level to be set to a depth of 16 mm above the cathode surface. With reference to equations 3 and 4, a voltage of –5.6 kV was therefore applied at the cathode, producing corresponding fields within the vapour phase below the THGEM of 4 kV/cm, and within the liquid of 2.5 kV/cm.

Measurements, shown in figure 8, were made of the charge gain as a function of the amplification field within the THGEM in 1 bar cold saturated argon gas above the liquid phase. For potential differences across the THGEM in excess of 2.7 kV, a photopeak was identified due to the internal 5.9 keV Fe-55 source, shown in figure 9. For a constant amplification field, these events were stopped by reduction of the drift field as shown in figure 10, thereby demonstrating that they originated from within the liquid. No corresponding improvement in the charge collection was observed as the potential between the cathode and the lower THGEM electrode was increased above stated values. Measurements shown in figure 10 are similar to previous measurements of extraction efficiency [31].

3.5 Cryogenic measurement of secondary scintillation generated within a THGEM in the vapour phase of a double phase argon system using a SiPM device

In order to replicate as closely as possible the experimental parameters used in section 3.3 the SiPM device, now with a breakdown voltage of 24.2 V at -189 °C [10] was operated at a bias voltage of 25.2 V corresponding again to an over-voltage of 1 V. The device was positioned as shown in figure 2, in 1 bar saturated argon vapour 10.5 mm above the liquid level. For a constant drift field of 2.5 kV/cm within the liquid phase, the electric field between the THGEM electrodes was steadily increased and the photoelectron pulse distribution produced by the SiPM within a 10 μs data acquisition time window recorded. The DCR at a bias voltage of 25.2 V has been measured as

2009 JINST 4 P04002

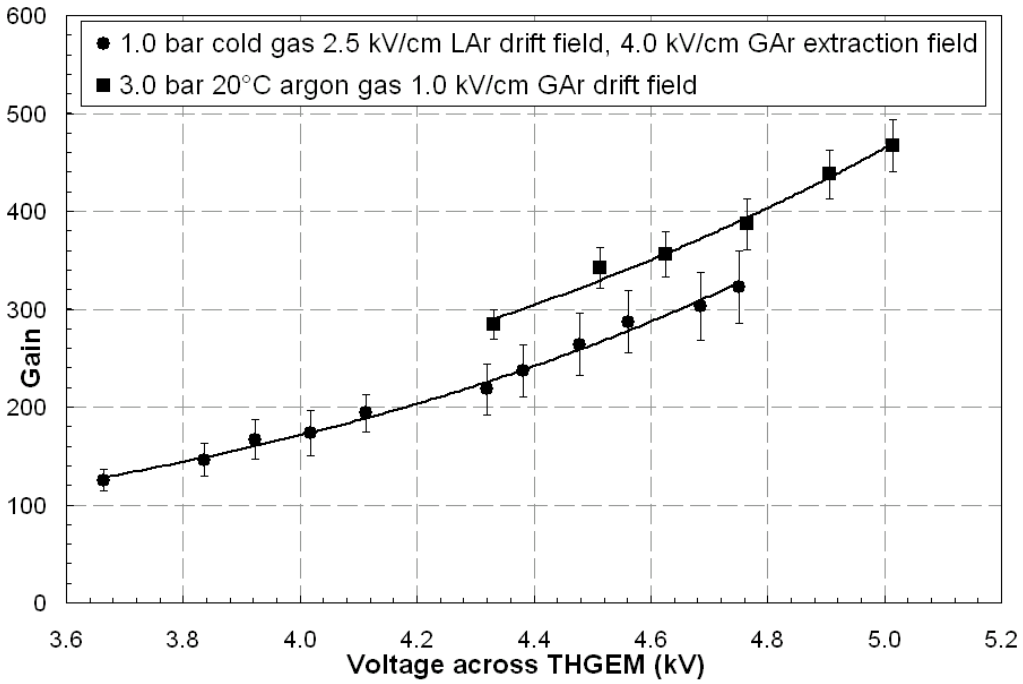

Figure 8. Charge gain versus potential across THGEM in 1 bar saturated argon gas above the liquid phase of a double phase system for a 2.5 kV/cm constant drift field within the liquid. Room temperature charge gain in 3 bar argon is shown for comparison.

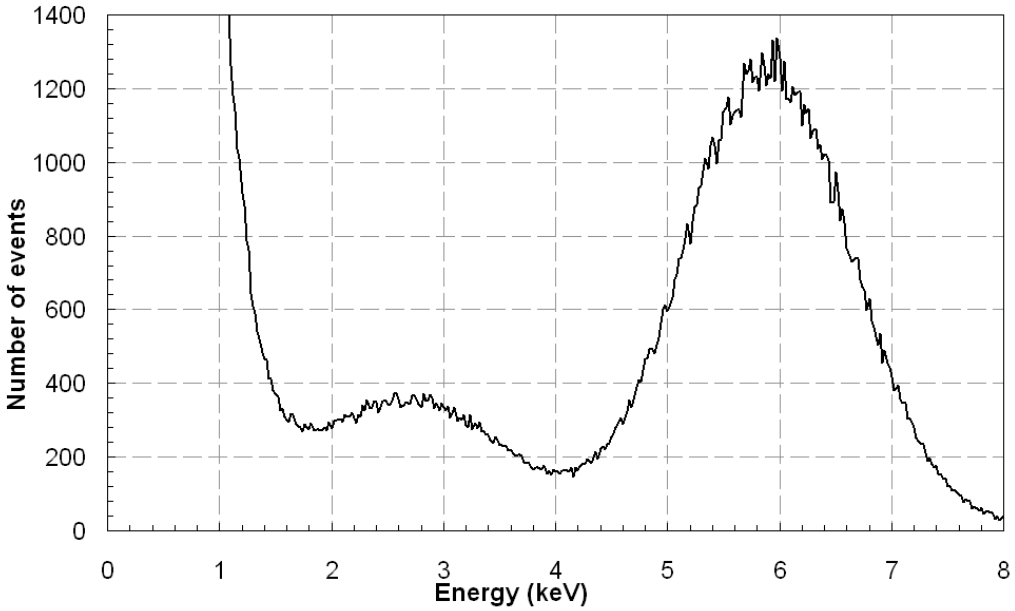

Figure 9. Charge spectrum from Fe-55 in the cold 1 bar gaseous argon phase of a double phase system. (V_{THGEM} = 4.685 kV, Drift field in liquid = 2.5 kV/cm and in gas = 4.0 kV/cm, gain = 303, 171388 total events.)

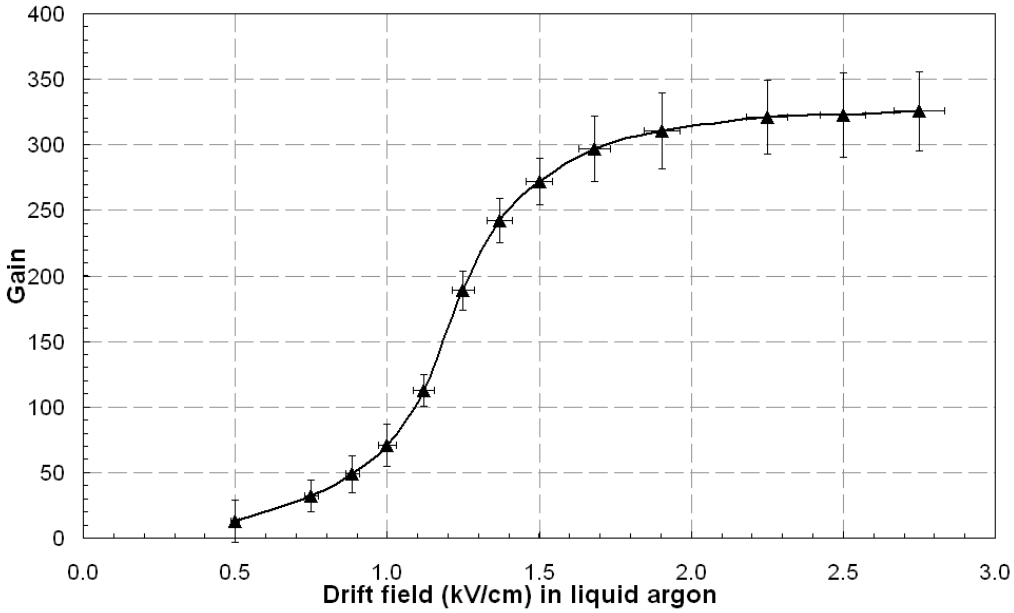

Figure 10. Charge gain versus drift field within liquid argon for a THGEM potential of 4.75 kV.

<30 Hz [10] and is therefore very unlikely to feature within a 10 μs window. The main contribution to the photoelectron background at zero field within the THGEM is again believed due to primary argon scintillation within the polystyrene tube providing an additional contribution at low energies.

As the field within the THGEM holes increased, secondary scintillation was observed between 2.1 kV and 3.4 kV. Figure 11 shows a secondary scintillation spectrum for Fe-55 for 2.16 kV across the THGEM, the presence of the argon escape peak (electron binding energy of 3.2 keV) providing calibration for the 5.9 keV Fe-55 peak. In all measurements the SiPM device was operated at an over-voltage of 1 V corresponding to a single photoelectron area of 0.5 Vns. Because of the digital nature of the SiPM output, each pulse will contain an integer number of single photoelectrons. For large SiPM pulses containing many photoelectrons small differences in the area of each photoelectron will cause a broadening of the total area. However for signals containing only a very small number of photoelectrons, the individual quantisation is still observed. This is evident in figure 11 for which a total of 12 spikes can be seen between the discriminator cut-off and the corresponding energy of 1 keV. Since the separation between the spikes is linked to the single photoelectron area an estimate of the number of photoelectrons corresponding to the 5.9 keV peak can be obtained. This is approximately 86 photoelectrons. Comparison with figure 9 reveals a lower noise threshold for operation in scintillation mode and slightly improved energy resolution at low applied voltages, as previously reported using an LAAPD / GEM combination to measure secondary scintillation light from xenon [26]. Figure 12 shows light collection as a function of THGEM voltage. Although a linear fit could be applied to the distribution, figure 8 suggests an exponential relationship to be more appropriate. Beyond 3.4 kV the rate of VUV photon production increased sharply with an associated worsening of the energy resolution until 3.75 kV at which point the saturation threshold of the SiPM device had been comprehensively exceeded and measurements were discontinued.

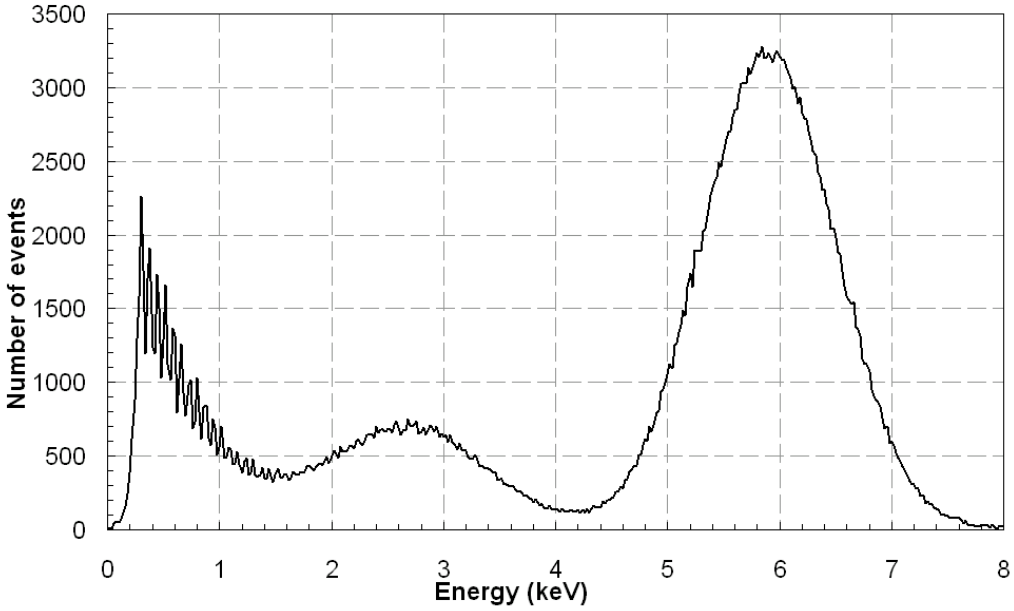

Figure 11. Secondary scintillation spectrum from Fe-55 in the cold 1 bar gaseous argon phase of a double phase system. (SiPM over-voltage=1 V, V_{THGEM} = 2.16 kV, Drift field in liquid = 2.5 kV/cm and in gas = 4.0 kV/cm, 5.9 keV peak corresponding to 86 photoelectrons, 361652 total events.)

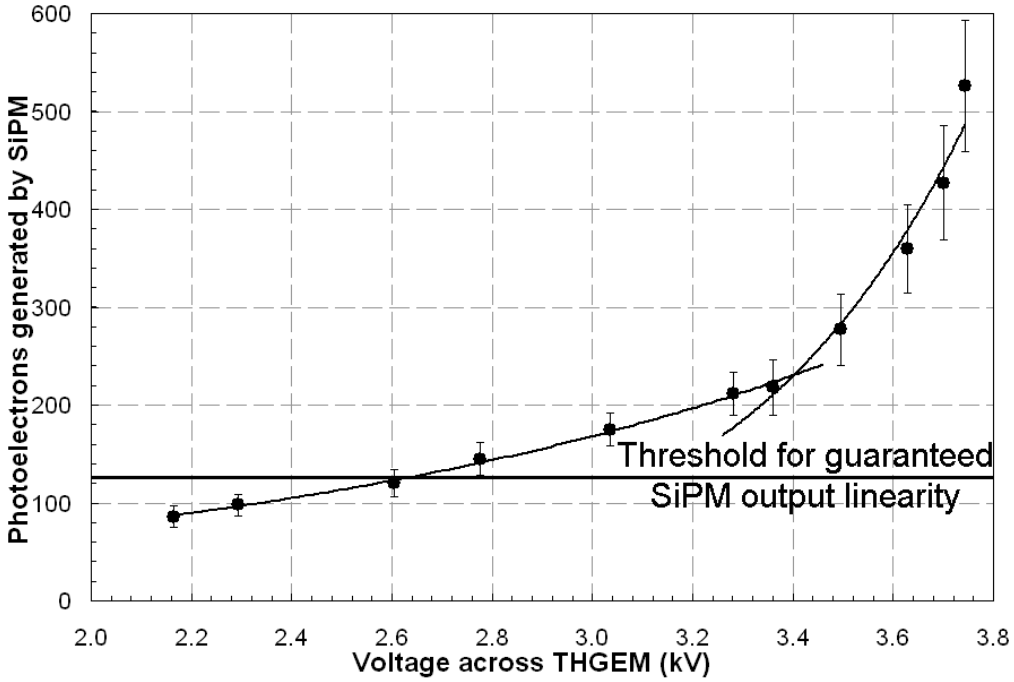

Figure 12. Secondary scintillation in 1 bar -189 °C gaseous argon as a function of the voltage across a THGEM due to the passage of charge generated via the interaction of an Fe-55 source in the liquid phase within a 2.5 kV/cm drift field.

2009 JINST 4 P04002

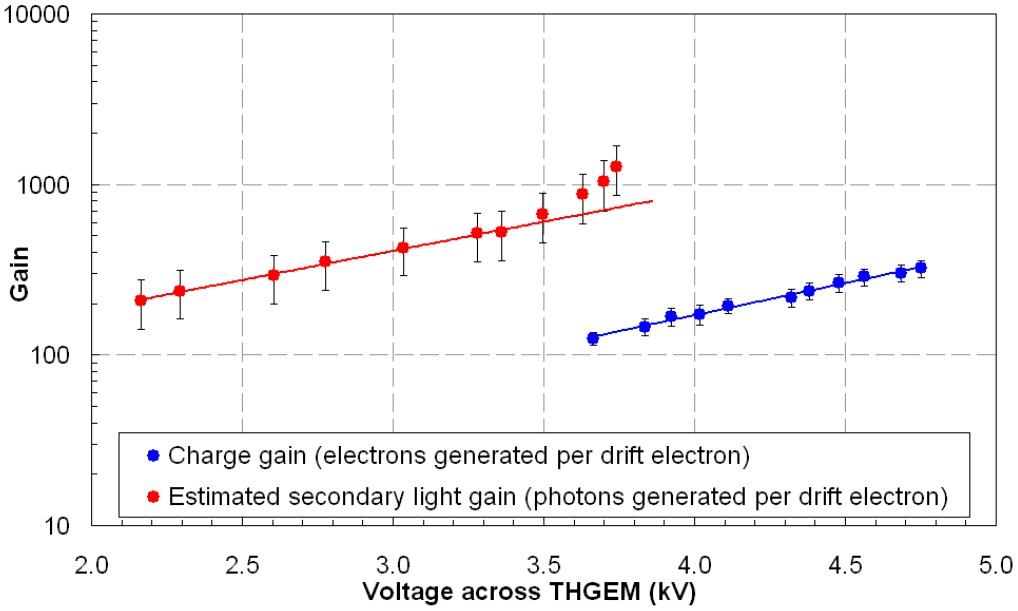

Figure 13. Estimated secondary scintillation gain and charge gain in the 1 bar cold gas phase of a double phase argon target as a function of voltage across the THGEM.

In figure 13, the maximum gain due to UV secondary scintillation can be compared with the charge gain as functions of voltage across the THGEM. Despite the crude approximation secondary scintillation is clearly initiated in advance of charge multiplication and consistently produces higher gains at comparable voltages. Ideally for a secondary scintillation based target, the field within the THGEM would be selected to be above the secondary scintillation threshold but below the electron impact ionisation threshold.

As already mentioned secondary scintillation is typically generated by the passage of charge through noble gas within a linear field [32]–[33]. The photon yield has been approximately characterised [25] by equation 5 below in which P is the gas pressure in bar, d is the drift distance in cm, and V is the potential difference in kV.

$$\text{Number of photons per drift electron } = 81\,(V - 0.58\,Pd) \tag{3.3}$$

It is therefore possible that proportional scintillation light may also be generated by any charge drifting between the SiPM protection grid and the top THGEM electrode, contributing to the total scintillation signal. With reference to equation 5, this may generate up to 189 photons per drifting electron.

It is therefore essential to confirm that the SiPM output signal is solely due to the secondary scintillation light generated within the THGEM by the passage of charge created by the gamma source within liquid argon. The presence of both the characteristic argon escape peak and Fe-55 full absorption peak in the correct ratio confirms that the collected light signal is predominantly due to argon scintillation. The origin of this signal can be gleaned from reducing the drift field as shown in figure 14. This shows the effect on secondary scintillation measured by the SiPM as the drift field within liquid argon is varied for a fixed THGEM potential of 3.36 kV. As the drift field within the

2009 JINST 4 P04002

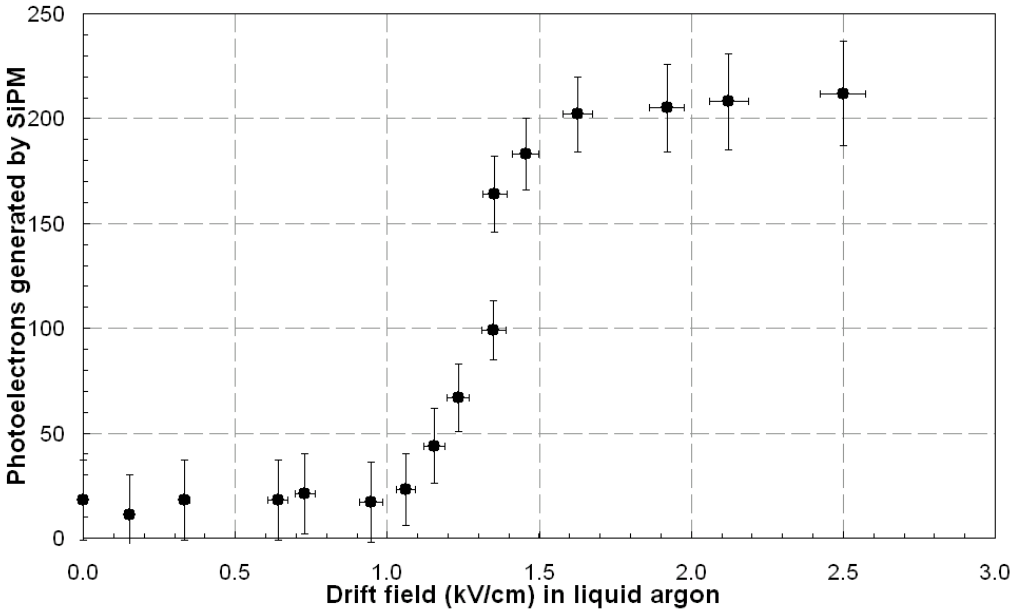

Figure 14. Secondary scintillation versus drift field within liquid argon for a fixed THGEM potential of 3.36 kV operating in the cold gas phase of a double phase target.

liquid is reduced from 2.5 kV/cm, light collection at the SiPM drops to 10% of its original value. A similar reduction in charge gain has already been observed as the drift field within the liquid was decreased for a constant amplification field as shown in figure 10. It is therefore concluded that the reduced drift field limits charge transfer within the drift region and that the light observed by the SiPM is as a direct consequence of the passage of this charge from the liquid argon through the THGEM. Any scintillation light generated between the protection grid and the top electrode of the THGEM would be unaffected by the variation in the drift field. It can therefore be stated that no clear contribution to the overall light signal is observed from the gaseous region between the protection grid and the THGEM and that the optical signal produced by the SiPM is due to the Fe-55 source.

3.6 Secondary scintillation generated within a THGEM measured using a SiPM device with both immersed in a single phase liquid argon system

Sections 3.4 and 3.5 successfully demonstrated both cryogenic operation of the SiPM device and successful charge transfer through purified liquid argon. Whilst charge amplification in cold argon vapour has already been successfully achieved in GEMs [34] and also in THGEMs [8, 9], exhaustive testing failed to generate any measurable charge gain from a THGEM submerged in liquid argon.

Following directly from double phase testing, liquefaction was continued until the combined capacitance of both level sensors reached 70 nF indicating that both the SiPM and THGEM were submerged. Filling was then discontinued and the target pressure maintained at 1 bar via adjustment of the pressure within the liquid nitrogen filled cryogenic jacket. In the absence of applied fields, pulses containing up to 50 photoelectrons were registered at the SiPM device, attributed to back-

2009 JINST 4 P04002

ground gamma interaction with liquid argon contained inside the polystyrene tube directly below the SiPM. During initial testing this tube had not been included in the design, resulting in the SiPM device being exposed to all incident primary scintillation light created inside the liquid argon cell. The addition of the tube isolated the SiPM and significantly reduced the background photoelectron contribution which had formerly masked the Fe-55 signal from the THGEM device. In addition the discrimination level for the trigger was adjusted to reduce the occurrence of low energy events. The drift field was set to 2.5 kV/cm and the voltage across the THGEM was slowly increased.

At voltages across the THGEM in excess of 8 kV the rate and magnitude of the scintillation pulses became more pronounced. As detailed earlier the output signal from the SiPM preamplifier was split, one signal passing directly to an input channel on the Acqiris unit. The other signal was connected through an Ortec 572 shaping amplifier with a 10 μs integration time, to a N417 discriminator and then to the trigger input of the Acqiris unit. Pulses containing few photoelectrons, when integrated by the shaping amplifier, corresponded to low output voltages passing into the discriminator unit. By careful adjustment of the discriminator threshold level, the Acqiris system was triggered only on signals containing more than a minimum number of photoelectrons. The absolute number of photoelectrons within a single pulse required to initiate a trigger was adjusted relative to the voltage across the THGEM and was selected based on both the output spectra, such as those shown in figures 16, 17 and 18, and also by observing single events such as that shown in figure 15. For example in figure 16 at a voltage across the THGEM of 9.91 kV the discriminator level was set to trigger only on events containing in excess of 10 photoelectrons. Quantisation of events containing small integer numbers of photoelectrons shown in figure 16 close to the discriminator cut off level illustrates this value. In figure 18 however at a voltage of 10.32 kV across the THGEM the higher occurrence of low energy events necessitated an increase in the discriminator level to a value corresponding to approximately 72 photoelectrons within the pulse.

In addition the integrated pulse was also passed through a low pass hardware filter, designed to veto events containing an extremely high number of photoelectrons. This low pass filter was employed only at very high amplification fields for which characteristic discharge sparking was observed. In data presented in figures 16, 17 and 18, the low pass filter was not used, although in measurements for which the voltage across the THGEM exceeded 10.5 kV, sporadic discharge sparking necessitated its use in order to veto events containing exceptionally high SiPM device saturating numbers of photoelectrons.

For a constant drift field of 2.5 kV/cm the voltage across the THGEM was gradually increased. At a voltage across the THGEM of 9.85 kV, a peak believed to be due to the Fe-55 source was observed. The low pass filter was not used to collect this data and the discriminator cut-off could be clearly seen to be distant from the peak attributed to the source. In addition reduction of the drift field resulted in complete removal of this peak from the output spectra. Figure 15 shows a characteristic pulse attributed to Fe-55 at 9.91 kV between the THGEM electrodes. Each individual event, such as that shown in figure 15, was recorded by the Acqiris data acquisition software and analysed separately. For each event a fit was made to the fast and slow component decay times and the total area of the pulse recorded. A spectrum was then produced such as that shown in figure 16. Because the output pulses contain integer numbers of photoelectrons, the spectrum shown in figure 16 shows quantised peaks containing between 10 and 16 photoelectrons per pulse between approximately 0.95 and 1.5 keV. In figure 16 for a drift field of 2.5 kV/cm and a potential difference across

2009 JINST 4 P04002

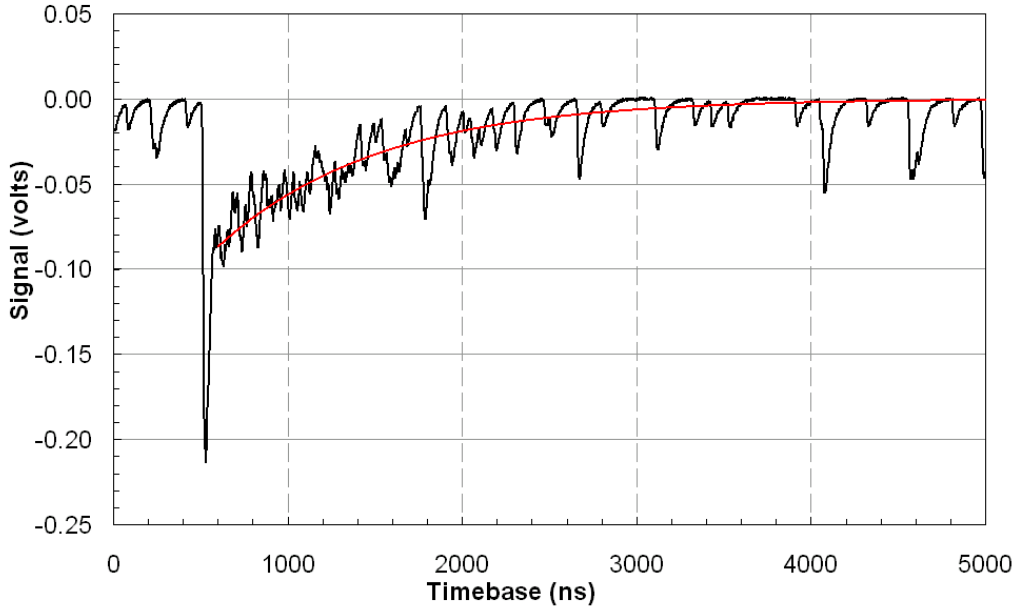

Figure 15. Example of a secondary scintillation light pulse produced by an Fe-55 source in a liquid argon system. (SiPM over-voltage=1 V, V_{THGEM} = 9.91 kV, Drift field in liquid = 2.5 kV/cm.)

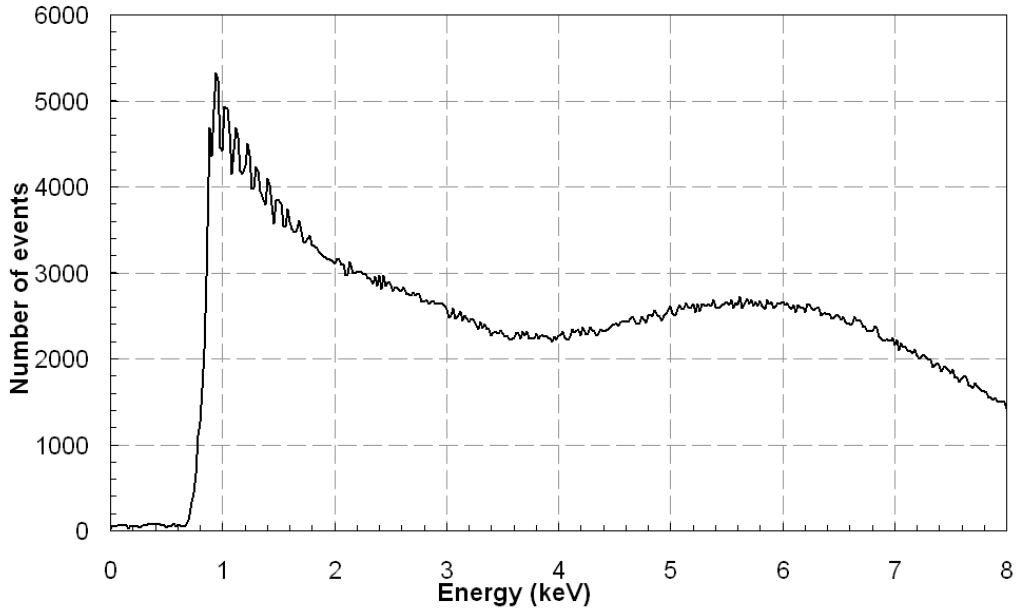

Figure 16. Secondary scintillation spectrum from Fe-55 in a liquid argon system. (SiPM over-voltage=1 V, V_{THGEM} = 9.91 kV, Drift field in liquid = 2.5 kV/cm, 5.9 keV peak corresponding to 62 photoelectrons, 1037508 total events.)

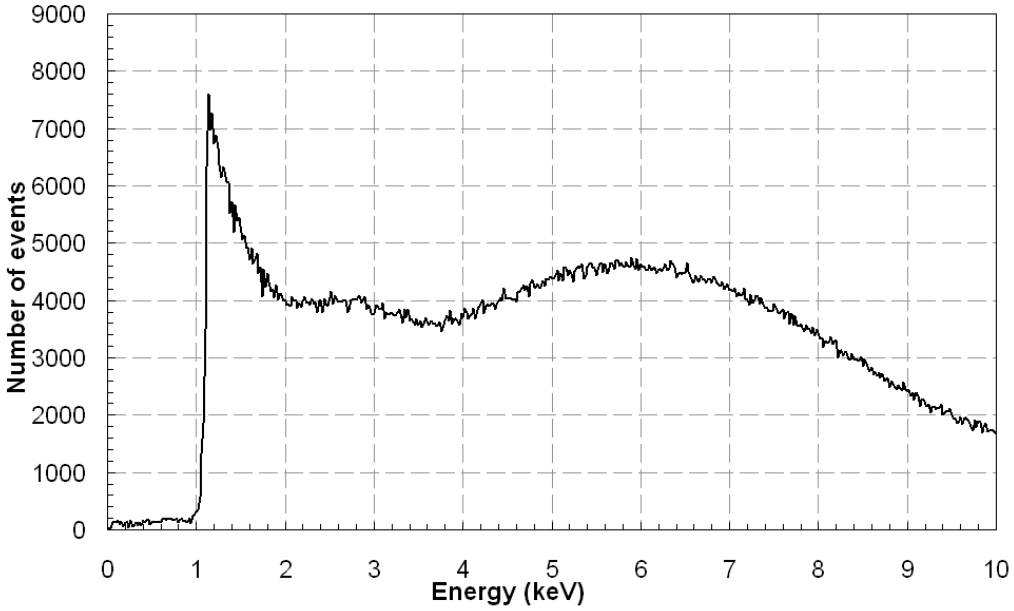

Figure 17. Secondary scintillation spectrum from Fe-55 in a liquid argon system. (SiPM over-voltage= 1 V, V_{THGEM} = 10.15 kV, Drift field in liquid = 2.5 kV/cm, 5.9 keV peak corresponding to 123 photoelectrons, 1721181 total events.)

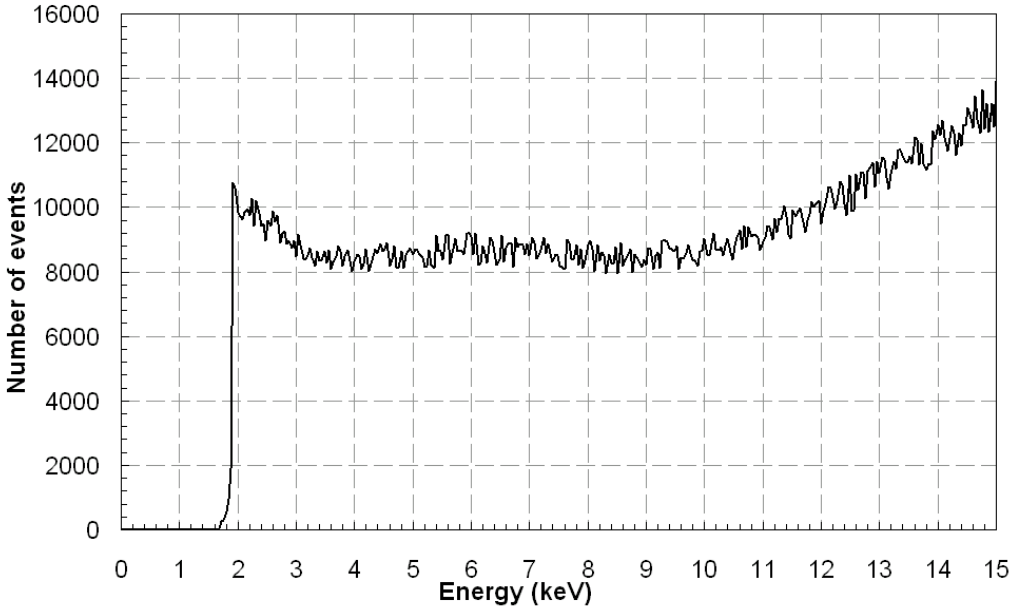

Figure 18. Secondary scintillation spectrum from Fe-55 in a liquid argon system. (SiPM over-voltage=1 V, V_{THGEM} = 10.32 kV, Drift field in liquid = 2.5 kV/cm, 5.9 keV energy level corresponding to 216 photoelectrons, 3398580 total events.)

2009 JINST 4 P04002

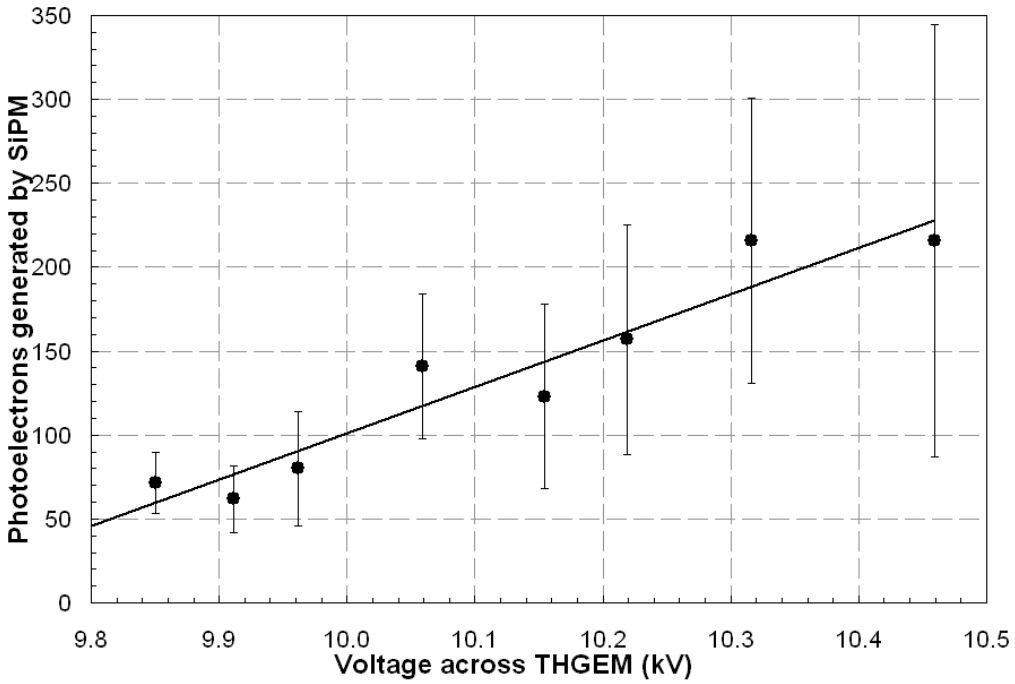

Figure 19. Secondary scintillation generated in liquid argon within a THGEM and viewed by a submerged SiPM device as a function of the voltage across a THGEM at a constant 2.5 kV/cm drift field.

the THGEM of 9.91 kV a peak is observed corresponding to an area equivalent to 62 photoelectrons. Figure 15 is given as an example of a single event which contributed to this peak distribution. Since this peak and a far less distinct peak corresponding to an area equivalent to 28 photoelectrons are absent for all data for which the drift field is removed, their origin is deemed to be the Fe-55 source and so an area corresponding to 62 photoelectrons is assigned an energy of 5.9 keV as shown in figure 16. This process was then repeated for different voltages across the THGEM.

As the voltage across the THGEM was increased the proportion of events containing discharge sparking also increased. Sparking could be distinguished from typical scintillation events because of the presence of significant albeit short lived current draw between the THGEM electrodes shown on the voltage supply, and also because of the characteristically shaped events displayed on the Acqiris on-line data analysis window. These events consisted of a very large area fast signal lasting no than 300 ns followed by multiple smaller area fast events. The increased presence of these events as the voltage across the THGEM was increased resulted in greater spread in the number of photoelectrons contained within each event leading to a loss in resolution until at 10.32 kV the peak became almost impossible to separate from the background contribution (see figure 18). Figure 19 shows the number of photoelectrons corresponding to the peak attributed to the Fe-55 source as a function of the voltage across the THGEM.

Since the discriminator cut-off in figure 17 is clearly separate from the peak attributed to Fe-55, and since this peak can be effectively removed from the spectrum by eliminating the drift field as illustrated in figure 20, it can be stated that this peak is as a result of the interaction of Fe-55. Section 3.5 clearly demonstrated passage of charge due to interaction of the Fe-55 source from the

2009 JINST 4 P04002

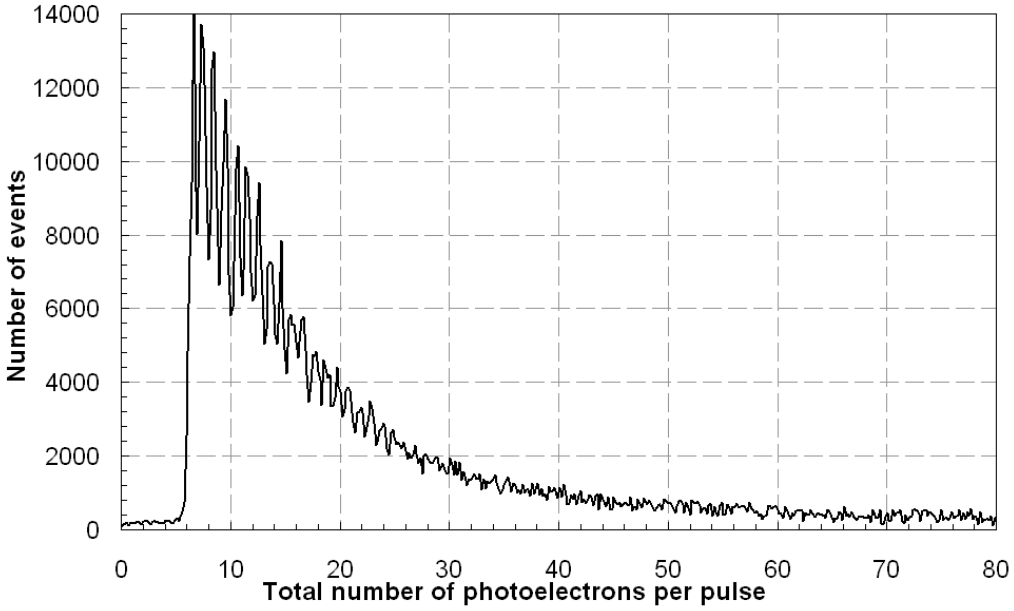

Figure 20. Secondary scintillation spectrum from Fe-55 in a liquid argon system. (SiPM over-voltage=1 V, V_{THGEM} = 10.15 kV, Drift field in liquid = 0 kV/cm, 932855 total events.)

drift region into the THGEM at which point secondary scintillation created by the THGEM was observed by the SiPM device. Figure 19 shows that the position of this peak increases linearly with increasing THGEM voltage as expected for secondary scintillation without charge amplification. However as the field within the THGEM is increased the resolution of the peak decreases as shown by comparison of figures 17 and 18, the proportion of events containing a high number of photoelectrons increasing. The Fe-55 peak position can be clearly followed for all data taken as the THGEM potential difference is increased from 9.85 kV to 10.22 kV, these voltages corresponding to a total number of 72 and 157 photoelectrons respectively within each pulse as shown in figure 19. For THGEM potential differences in excess of 10.22 kV an additional contribution is observed, clearly evident in figure 18 above 10 keV which reduces the resolution of the Fe-55 peak. Figure 18 has been included in this report to identify the upper threshold of reliable operation of the apparatus rather than as definitive proof of principle for secondary scintillation in liquid argon. In order to improve energy resolution of future devices the origin of this additional contribution must be identified.

Prior to the application of both the drift and amplification fields, pulses containing up to 50 photoelectrons were registered at the SiPM device, attributed to background gamma interaction with liquid argon contained inside the polystyrene tube directly below the SiPM. During initial testing this tube had not been included in the design, resulting in the SiPM device being exposed to all incident primary scintillation light created inside the liquid argon cell. The addition of the tube isolated the SiPM and significantly reduced the background photoelectron contribution which had formerly masked the Fe-55 signal from the THGEM device. This was a key step in allowing the Fe-55 signal to be observed. The additional contribution above 10 keV evident in figure 18 is absent from figure 16 and also from all data for which the THGEM was operated at a voltage

2009 JINST 4 P04002

below 10.22 keV. It must therefore be concluded that the additional effect in figure 18 above 10 keV is not due to primary scintillation light from argon, but is as a direct result of increasing the amplification field within the THGEM. In previous measurements for which the THGEM was operated in room temperature and cryogenic argon gas, a significant increase in the number of photoelectrons within each event was observed as the sparking threshold was reached. The long integration window of 10 μs needed to capture a scintillation event in liquid argon also has the effect of recording a substantial number of photoelectrons generated from sources other than the passage of Fe-55 charge through the THGEM hole. In the fitting process this causes a significant increase in the number of photoelectrons observed and for high THGEM voltages a total loss of the peak believed to be associated with Fe-55. This peak is clear from 9.85 kV to 10.22 kV and is only lost at the onset of severe sparking. It is imagined that corona discharge from local field instabilities caused by mechanical artefacts within the THGEM hole lead to positive photon feedback eventually culminating in premature breakdown. Field instabilities may also be responsible for the narrow operating regime of the device at high voltage, and excessive photon feedback effects are widely held to be a fundamental reason significant charge gain has been unattainable using micropattern devices in liquid noble gases.

At any time a proportion of the total number of pixels of the SiPM device will be in a state of recovery, the fraction dependent on the intensity and frequency of the photon flux. This characteristic places a limit on the extent of linearity of the device especially for high intensity pulses of similar frequency to the pixel recovery time because photons incident on a pixel in a state of only partial recovery will not be registered. For electron recoils within liquid argon approximately 23% of all photons [22] are produced within the first 6 ns following an interaction, the remaining 77% forming an exponential distribution with a 1590 ns time constant [20]. In contrast for room temperature gaseous argon, it has been deduced by analysis of the data contained in this report, that approximately 67% of all photons are produced within the first 11.3 ns the remaining 33% forming an exponential distribution with a 3140 ns time constant as detailed in table 2. The 40 ns pixel recovery time of the SiPM device implies that loss of output linearity is more likely for pulses containing a high proportion of photoelectrons within the fast component. Since scintillation from gaseous argon contains proportionally far more photoelectrons in the fast component, output linearity from the SiPM is lost for events containing a lower total number of photoelectrons when compared with scintillation events from liquid argon. The threshold for SiPM device linearity in liquid argon was again determined by the point at which 84 photoelectrons occurred within a 40 ns pulse window (see figure 3). Since the number of photoelectrons contained within the slow component is triple the number within the fast 6 ns component for electron recoils in liquid argon [22], the linear range of the device is effectively extended compared with operation in argon gas for which the fast component dominates. Therefore the linearity of the SiPM device was not exceeded in all data shown.

Comparison of data shown in figures 11 and 16 shows the resolution of the Fe-55 signal is also degraded in liquid compared to measurements taken in cold gaseous argon attributed to the 10 μs integration time required to fully acquire the slow component time constant of 1590 ns [20]. Since the software records all photoelectrons generated within this long time window the data will most likely contain in addition to an Fe-55 pulse, contributions from primary scintillation due to background interaction with liquid argon contained within the polystyrene tube, DCR effects generated by the SiPM device, and also photons created due to sparking within the THGEM operating

2009 JINST 4 P04002

close to the breakdown threshold. Since the temperature of the SiPM device is identical for data presented in figures 11 and 16 the DCR is also equal. Because of the increased density of the liquid argon contained within the polystyrene tube in comparison to the gaseous argon present in a cold double phase system, energy deposition by background gammas for example is increased. This creates a greater contribution to the total pulse area when the amplification and drift fields are removed. As has already been mentioned at high voltages across the THGEM discharge sparking occurs which generates large number of photoelectrons. This also contributes to the overall number of photoelectrons contained within each event.

In all measurements for which both the THGEM and the SiPM device were immersed in liquid argon, a drift field of 2.5 kV/cm was applied between the lower electrode of the THGEM and the cathode. This value had been selected based on data presented in figures 9 and 10. Figure 9 clearly illustrated that charge created in liquid argon following the interaction of Fe-55 had been successfully transferred through the drift region and amplified within the THGEM. Figure 10 demonstrated the effect of decreasing the drift field within liquid argon, fields at least in excess of 1.5 kV/cm required to ensure efficient charge transfer. For this reason a drift field of 2.5 kV/cm was selected for all single phase liquid tests.

In the same manner in which it had been demonstrated in figure 14 that scintillation pulses recorded by the SiPM had been generated by charge originating within the drift region following the interaction of Fe-55, the drift field was reduced from 2.5 kV/cm, and the effect on the energy spectra measured at the SiPM recorded for two applied voltages across the THGEM. Figure 17 illustrates the energy spectrum created for a potential difference of 10.15 kV across the THGEM, and for a drift field in liquid of 2.5 kV/cm. A distinct albeit poorly resolved peak is evident at an energy of 5.9 keV corresponding to a pulse containing a total of 123 photoelectrons. A second far less distinct peak is present at an energy of approximately 2.7 keV corresponding to a pulse containing a total of 56 photoelectrons. Unlike figure 16 no quantisation of the spectrum due to the digital nature of the SiPM output is observed for pulses containing a low number of photoelectrons.

Figure 20 shows the total pulse area spectrum related to a potential difference of 10.15 kV across the THGEM for which there is no corresponding drift field in the liquid. In previous spectra the calibration between energy and total pulse area has been made based on the presence of a characteristic peak assumed to represent 5.9 keV. In figure 20 no such peak is evident and the calibration cannot be made. Instead the total number of photoelectrons in each pulse is plotted. Quantisation of total pulse area due to the digital nature of the SiPM device is clearly observed for pulses containing between 8 and 25 photoelectrons. Digitisation also allows a comparison to be made with data presented in figure 17 for which a clear peak is observed for pulses containing 123 photoelectrons. This is clearly absent from figure 20 although the over-voltage at the SiPM and the voltage across the THGEM are identical. Only the drift field in liquid argon is absent. It must therefore be concluded that the population of events contributing to the peak at 123 photoelectrons in figure 17 is due to the Fe-55 source.

Figure 21 illustrates the effect on the presumed Fe-55 peak position in the energy spectra and its resolution as the drift field is reduced. Pulses were recorded for voltages across the THGEM of 9.91 kV and 10.15 kV. Since both were lower than 10.32 kV - the voltage above which sporadic discharge causes a large increase in photon production leading to saturation of the SiPM and concealment of the peak attributed to the source - the peak position and resolution could be easily

2009 JINST 4 P04002

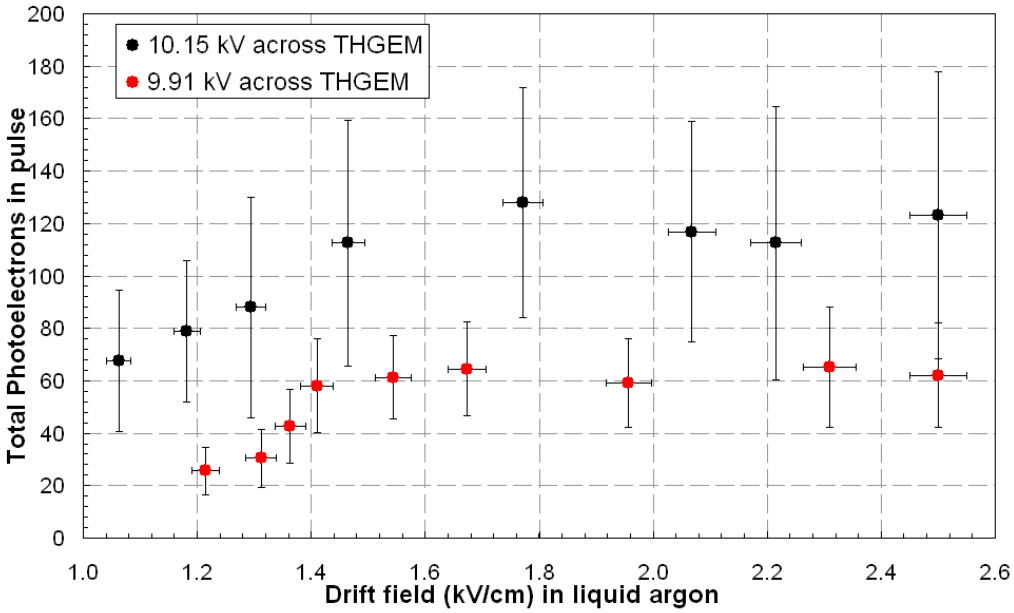

Figure 21. Secondary scintillation corresponding to the Fe-55 peak versus drift field within liquid argon for fixed THGEM potentials of both 9.91 kV (red) and 10.15 kV (black).

determined. In both cases as the drift field was reduced no variation of either the peak position or the resolution were noted between 2.5 kV/cm and 1.5 kV/cm outside errors. For data taken at a voltage across the THGEM of 9.91 kV the number of photoelectrons corresponding to the peak attributed to the source decreased for drift fields below 1.4 kV/cm. As the drift field was reduced still further, the number of photoelectrons quickly decreased and eventually the peak believed due to Fe-55 was subsumed into the background. At this point a comparative measure of charge transfer through liquid argon could not be determined, the effect of the Fe-55 source could not be observed, and an energy calibration could no longer be made.

The same characteristics were noted for data taken at a voltage of 10.15 kV across the THGEM. Since the amplification field within the THGEM was greater, the number of photoelectrons corresponding to the presumed Fe-55 peak was larger. As the drift voltage reduced from 1.5 kV/cm to 1.0 kV/cm, the number of photoelectrons constituting the total pulse area also decreased at a near linear rate until the peak became obscured by the exponential slope of low energy contributions. Data points marked on figure 21 identify the total number of photoelectrons within a pulse corresponding to the centre of the peak due to the presence of the Fe-55 source. Only measurements for which the peak could be clearly discerned from the remainder of the spectrum were included.

The point at which the peak attributed to Fe-55 can no longer be resolved in the energy spectrum is dependent not only on the extent with which the charge transfer efficiency through liquid argon reduces with decreasing drift field, but also on the intensity of background scintillation events within liquid argon detected by the SiPM. In figures 10 and 14 the drift field is quoted specifically as being in the liquid phase. Since operation in single phase liquid argon immediately followed double phase testing, we can directly compare data. Reduction of the drift field at a constant amplification field results in a decrease in the drift velocity of charge and an alteration of the focussing

2009 JINST 4 P04002

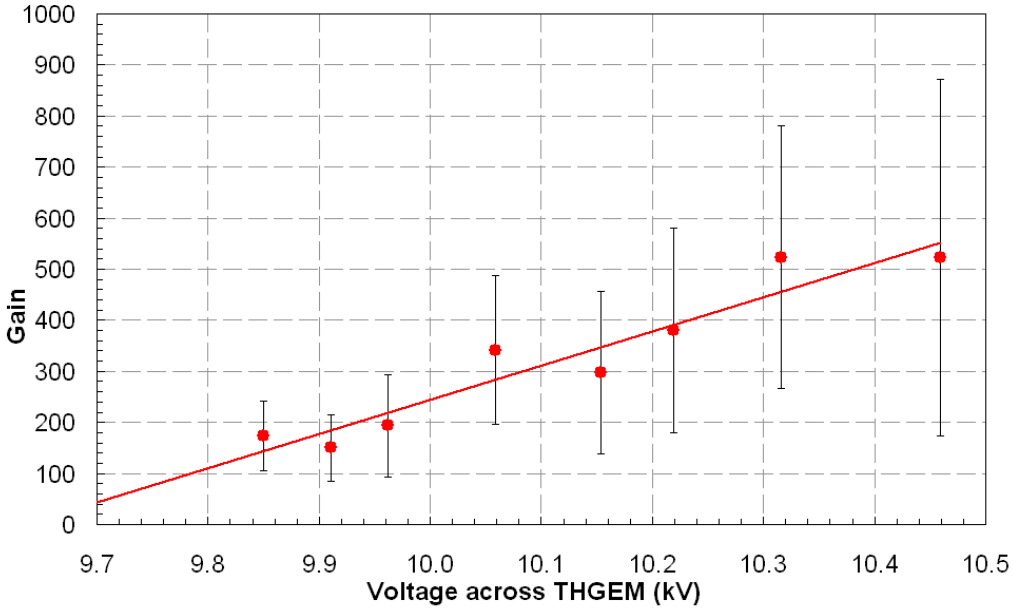

Figure 22. Estimated secondary scintillation gain in liquid argon as a function of voltage across the THGEM.

of field lines passing from the drift region through the THGEM. Data presented in figure 10 to illustrate charge transfer efficiency as a function of drift field in liquid argon was taken for a voltage across the THGEM of 4.75 kV in cold gaseous argon whereas data in figure 21 is for voltages in excess of 9.91 kV in liquid. Nonetheless similarities exist between the figures. In both, the initial drop in charge or light respectively is observed for a drift field of approximately 1.5 kV/cm. Data in figure 10 indicates that charge transfer efficiency reduces to approximately 23% of its original value as the drift field is reduced from 2.5 kV/cm to 1.0 kV/cm. Although this includes extraction from the liquid surface into the gas phase, and therefore cannot be directly compared to data taken in single phase liquid, it may be suggested that at a drift field of 1.0 kV/cm in figure 21, a non-zero quantity of charge is successfully transferred through the liquid giving rise to the data shown for a THGEM potential of 10.15 kV.

Finally an estimate was made of the absolute photon yield produced at the THGEM. This was calculated in the same way as had been done for figure 13 based on the number of photons observed at the SiPM due to the Fe-55 source and the approximate efficiency of detection of the original photon emission at the THGEM. The scintillation yield in terms of photons generated at the THGEM per drifting electron as a function of the voltage between the electrodes is shown in figure 22. Unlike figure 13, no comparison can be made with the charge gain since charge gain within a THGEM has not at present been observed in liquid argon.

4 Discussion

Studies of charge amplification [6, 13] in pure liquid argon have failed to yield any reliable gain. Irrespective of the choice of charge readout device, the maximum charge gain drops with increasing gas pressure and therefore density [35]. The exact reason for this is not well established. In

2009 JINST 4 P04002

addition to effects caused by the elevated high voltage on the detector's electrodes, it is likely that the Raether limit may also contribute to the gain limit. This was recently demonstrated experimentally [36]. Decrease in maximum charge gain has also been noted in cryogenic gas with increased density as demonstrated within this report and also using cascaded GEMs [34, 37] and resistive electrode thick gas electron multipliers (RETGEMs) [34].

Although the breakdown limit of a THGEM operating in charge gain mode in pure noble gas is ultimately determined by the effect of UV photon emission, in a heavily optimised system gain is limited by charge build up within the amplification region. The high electric fields required for charge amplification can also lead to charging of the dielectric and ultimately to dielectric breakdown. Additionally, high levels of UV photon emission (secondary scintillation) always associated with charge gain, reduce the device stability, and bubble formation on the sharp edges of the THGEM electrodes can lead to the creation of conducting paths [6] culminating in gaseous discharge.

Secondary scintillation was only observed in gas at THGEM fields for which charge amplification was already established, with the effect that ionisation electrons created in the charge multiplication process then interacting with the medium, yield additional secondary scintillation and therefore an exponential scaling with the applied field. No evidence of charge multiplication was detected during this work for any electric field within liquid argon and it is assumed that the field required to initiate secondary scintillation via excitation is below the ionisation threshold of the medium, the energy dissipated via the emission of UV photons, which do not participate further in the process. Secondary scintillation therefore scales linearly with electric field in the liquid, and may therefore eventually be considered more predictable and less prone to breakdown. Results contained within this report have demonstrated that using secondary scintillation as the readout signal, high gains are possible. Satisfactory energy resolution has not as yet been achieved from a single THGEM in liquid argon. The results detailed within this report are intended to demonstrate proof of principle and it is believed that energy resolution may be improved by optimisation of the experimental parameters such as the THGEM hole profile, the solid angle of light collection, and the thickness of the waveshifting gel applied to the SiPM. By operating the THGEM at a lower field in the secondary scintillation proportional mode, detector instability is reduced, and dielectric and UV photon mediated breakdown are avoided. Readout of secondary scintillation also increases signal to noise ratio and reduces the requirements of the front end electronics on the THGEM.

High purity is crucial for any measurement connected to charge transfer through liquid argon. The chemical purification blends and techniques detailed within this report were originally developed for use in the 1 tonne Argon Dark Matter experiment (ArDM) for which charge transfer lengths of up to 1m in liquid argon are a requirement. Charge transfer measurements have been carried out within the apparatus shown in figure 1 over distances from 2 cm to 10 cm within liquid argon, with no degradation of the signal within errors. Gas purity can be ascertained from the fit made to the triplet decay time [21] of scintillation pulses. In all previous measurements purity has remained constant throughout the period for which measurements were taken, and such is the lifetime of the purification cartridge shown in figure 1, that it is not routinely replaced upon removal of liquid argon from the apparatus. Figure 9 clearly substantiates charge transfer through liquid argon and so long as the purity remains constant between measurements, the data can be directly compared irrespective of the absolute value of electron lifetime in the liquid.

2009 JINST 4 P04002

5 Conclusions

For the first time secondary scintillation, generated within the holes of a thick gas electron multiplier (THGEM) immersed in liquid argon, has been observed and measured using a silicon photomultiplier device (SiPM). Secondary scintillation has also been observed in room temperature gaseous argon and in 1 bar cold saturated vapour in a double phase chamber. In all cases the origin of the photon production was ascertained by reduction of the drift field. In order to explain the exponential nature of secondary scintillation generation, measurements of charge gain were taken in gaseous argon, comparison of the voltage range across the THGEM for each process revealing the resulting scintillation gain to be a combination of both.

The combination of the waveshifter tetraphenyl butadiene (TPB) within a gel applied to the surface of the SiPM device was found to efficiently absorb 128 nm VUV light produced within the THGEM holes, and to then emit 460 nm in the high quantum efficiency region of the device. Overall, for a SiPM over-voltage of 1 V, a THGEM voltage of 9.91 kV, and a drift field of 2.5 kV/cm, a total of 62 $\pm$ 20 photoelectrons were produced at the SiPM device per Fe-55 event, corresponding to an estimated gain of 150 $\pm$ 66 photoelectrons per drifted electron.

This new liquid argon detection technology is considered to hold great potential on the route to cost-effective, large volume, simultaneous tracking and calorimetry targets with excellent performance relevant to important applications in fundamental particle physics.

Acknowledgments

The authors would like to thank SensL Technologies Ltd. for their support during this project.

References

[1] ICARUS collaboration, S. Amerio et. al., *Design, construction and tests of the ICARUS T600 detector*, *Nucl. Instrum. Meth.* **A 527** (2004) 329.

[2] F. Sauli, *GEM: a new concept for electron amplification in gas detectors*, *Nucl. Instrum. Meth.* **A 386** (1997) 531.

[3] A. Breskin et. al., *A concise review on THGEM detectors*, *Nucl. Instrum. Meth.* **A 598** (2009) 107 and references therein.

[4] P.K. Lightfoot, R. Hollingworth, N.J.C. Spooner and D. Tovey, *Development of a double-phase Xenon cell using MicrOMEGAs charge readout for applications in dark matter physics*, *Nucl. Instrum. Meth.* **A 554** (2005) 266.

[5] P.K. Lightfoot, N.J.C. Spooner, T.B. Lawson, S. Aune and I. Giomataris, *First operation of bulk micromegas in low pressure negative ion drift gas mixtures for dark matter searches*, *Astropart. Phys.* **27** (2007) 490.

[6] J.G. Kim et. al., *Electron avalanches in liquid argon mixtures*, *Nucl. Instrum. Meth.* **A 534** (2004) 376.

[7] L. Periale et. al., *A study of the operation of especially designed photosensitive gaseous detectors at cryogenic temperatures*, *Nucl. Instrum. Meth.* **A 567** (2006) 381.

2009 JINST 4 P04002

[8] V. Peskov et. al., *Development and first tests of GEM-like detectors with resistive electrodes*, *IEEE Trans. Nucl. Sci.* **54** (2007) 1784.

[9] A. Bondar et. al., *Thick GEM versus thin GEM in two-phase argon avalanche detectors*, 2008 *JINST* **3** P07001.

[10] P.K. Lightfoot, G.J. Barker, K. Mavrokoridis, Y.A. Ramachers and N.J.C. Spooner, *Characterisation of a silicon photomultiplier device for applications in liquid argon based neutrino physics and dark matter searches*, 2008 *JINST* **3** P10001.

[11] S. Himi, T. Takahashi, J.z. Ruan and S. Kubota, *Liquid and solid argon, and nitrogen doped liquid and solid argon scintillators*, *Nucl. Instrum. Meth.* **203** (1982) 153.

[12] L.S. Miller, S. Howe and W.E. Spear, *Charge transport in solid and liquid Ar, Kr and Xe*, *Phys. Rev.* **166** (1968) 871.

[13] S.E. Derenzo, T.S. Mast, H. Zaklad and R.A. Muller, *Electron avalanche in liquid xenon*, *Phys. Rev.* **A 9** (1974) 2582.

[14] D.W. Swan, *Drift velocity of electrons in liquid argon, and the influence of molecular impurities*, *Proc. Phys. Soc. Lond.* **83** (1964) 659.

[15] S. Amoruso et. al., *Analysis of the liquid argon purity in the ICARUS T600 TPC*, *Nucl. Instrum. Meth.* **A 516** (2004) 68.

[16] E. Aprile, K.L. Giboni and C. Rubbia, *A study of ionization electrons drifting large distances in liquid and solid argon*, *Nucl. Instr. Meth.* **A 241** (1985) 62.

[17] T.W. Barnard et al., *Solid-state detector for ICP-OES*, *Anal. Chem.* **65** (1993) 1231.

[18] K. Mavrokoridis et al., *Development of wavelength shifter coated reflectors for the ArDM argon dark matter detector*, awaiting submission to JINST.

[19] M. Miyajima et. al., *Average energy expended per ion pair in liquid argon*, *Phys. Rev.* **A 9** (1974) 1438.

[20] A. Hitachi et. al., *Effect of ionization density on the time dependence of luminescence from liquid argon and xenon*, *Phys. Rev.* **B 27** (1983) 5279.

[21] C. Amsler et. al., *Luminescence quenching of the triplet excimer state by air traces in gaseous argon*, 2008 *JINST* **3** P02001.

[22] P. Benetti et al., *First results from a dark matter search with liquid argon at 87 K in the Gran Sasso underground laboratory*, *Astropart. Phys.* **28** (2008) 495.

[23] J.W. Keto, R.E. Gleason Jr and G.K. Walters, *Production mechanisms and radioactive lifetimes of argon and xenon molecules emitting in the ultraviolet*, *Phys. Rev. Lett.* **33** (1974) 1365.

[24] J.S. Kapustinsky, R.M. DeVries, N.J. DiGiacomo, W.E. Sondheim, J.W. Sunier and H. Coombes, *A fast timing light pulser for scintillation detectors*, *Nucl. Instrum. Meth.* **A 241** (1985) 612.

[25] C.M.B. Monteiro, J.A.M. Lopes, J.F. C.A. Veloso and J.M.F. dos Santos, *Secondary scintillation yield in pure argon*, *Phys. Lett.* **B 668** (2008) 167.

[26] A.S. Conceicao et. al., *GEM scintillation readout with avalanche photodiodes*, 2007 *JINST* **2** P09010.

[27] P.K. Lightfoot, K. Mavrokoridis and N.J.C. Spooner, *Characterisation of the electric field within an optical readout tracking detector concept using secondary scintillation from liquid argon generated by a thick gas electron multiplier*, awaiting submission to JINST.

2009 JINST 4 P04002

[28] A.I. Bolozdynya, *Two-phase emission detectors and their applications*, *Nucl. Instrum. Meth.* **A 422** (1999) 314.

[29] B.A. Dolgoshein et al., *New method of registration of ionizing-particle tracks in condensed Matter*, *JETP Lett.* **11** (1970) 513.

[30] A.F. Borghesani, G. Carugno, M. Cavenago and E. Conti, *Electron transmission through the Ar liquid-vapor interface*, *Phys. Lett.* **A 149** (1990) 481.

[31] E.M. Gushchin, A.A. Kruglov and I.M. Obodovskii, *Emission of 'hot' electrons from liquid and solid argon and xenon*, *Sov. Phys. JETP* **55** (1982) 860.

[32] G.J. Alner, et al., *Status of the ZEPLIN II experiment*, *New Astron. Rev.* **49** (2005) 259.

[33] C.M.B. Monteiro et. al., *Secondary Scintillation Yield in Pure Xenon*, 2007 *JINST* **2** P05001.

[34] A. Bondar et. al., *Two-phase argon and xenon avalanche detectors based on Gas Electron Multipliers*, *Nucl. Instrum. Meth.* **A 556** (2006) 273.

[35] F.D. Amaro et. al., *Operation of a single-GEM in noble gases at high pressures*, *Nucl. Instrum. Meth.* **A 579** (2007) 62.

[36] A. Di Mauro et. al., *GEMs with Double Layred Micropattern Electrodes and their Applications*, arXiv:0811.4120.

[37] V. Solovov, F. Balau, F. Neves, V. Chepel, A. Pereira and M.I. Lopes, *Operation of gas electron multipliers in pure xenon at low temperatures*, *Nucl. Instrum. Meth.* **A 580** (2007) 331.

2009 JINST 4 P04002